１．研究課題名：

高速光計測法

２．研究機関：

電子技術総合研究所

３．研究者名と所属　：

高島一郎（電子技術総合研究所 超分子部）

４．研究協力者名と所属：

飯島敏夫（電子技術総合研究所 超分子部）
梶原利一（電子技術総合研究所 超分子部）
菰淵寛仁（松下電器産業(株) 先端技術研究所 次世代デバイス研究グループ）
森中康弘（松下電器産業(株) 先端技術研究所 次世代デバイス研究グループ）

５．研究期間：1996 年―2000 年

６．要約

脳の神経活動ならびに代謝活動をリアルタイムで高速イメージングするための高速光計測法の研究開発を行った。研究期間中、以下の仕様を有する光計測装置を完成させた。(1)ＣＣＤ撮像素子を使用(1/3 インチサイズの市販品 および 1.2 インチサイズのカスタム品)、(2)ショットノイズ S/N が 68dB 以上、(3)毎秒 300～1300 フレームの撮像レート、(4)１インチサイズ撮像素子面に均一光量(>95%)を確保する光学系、(5)ウィンドウズベースＧＵＩの計測ソフトウェア。 開発した計測装置を用いれば、(A)膜電位感受性色素由来の外因性光シグナル(１次シグナル)、(B)組織の酸素消費/局所血液量変化由来の内因性光シグナル(２次シグナル)、の両方を高解像度、高感度、高 S/N で記録できることを示した。さらに、同一動物個体標本から１次シグナルによる神経活動マップと２次シグナルによる代謝活動マップを記録し、両者を定量的に比較解析する手法の確立を行った。

７．研究目的

我々が記録し得る脳活動由来のシグナルは、１次シグナルと２次シグナルに大別できる。１次シグナルは神経興奮そのもののシグナル（膜電位変化や膜電流変化）であり、２次シグナルは神経活動変化にカップルした神経組織の代謝変動に由来するシグナルである。２次シグナルは、ｆＭＲＩやＰＥＴにより無侵襲的に脳の広域空間から同時計測できる点で脳の活動部位の推定に有用であるが、１次シグナルとの関係（例えば、時間経過、空間的広がり）は未だ明らかでない。

高速光計測法では、撮像デバイスにより脳表面からのわずかな光量変化を捉えることで、１次シグナルと２次シグナルの両方を検出し、イメージングすることができる。しかしながら従来、この１次シグナルと２次シグナルはその応答時間、測定光波長の

違いから、異なる光計測システムを用いて別々に記録され、その直接の比較は困難であった。そこで本研究では、同一個体標本から、１次シグナルによる神経活動マップと２次シグナルによる代謝活動マップを得て、両者を定量的に比較解析するための、新しい光計測装置と計測手法の研究開発を行う。

８．材料と方法

1) 光計測装置タイプ１

本光計測装置は、小動物を測定対象とし、市販の 1/3 インチサイズＣＣＤチップをコアに開発した。装置はカメラモジュールとプロセッサユニットから構成される。カメラモジュールは 5x5x9 cm, 225 g と軽量コンパクトであり、Ｃマウントアダプタで顕微鏡に取り付け可能である。一方、プロセッサユニットは、PC/AT コンピュータに装着された 16 ビット ISA インターフェースカードを介して制御される（図１）。

図１　光計測装置タイプ１の概観

[カメラモジュール]　ＣＣＤチップの画素数は 512x492、インターライン転送方式、垂直方向電荷転送は４相クロック制御である。ＣＣＤの駆動に必要なハードウェアロジックはＦＰＧＡ(Field Programmable Gate Array)デバイスを用いて実現した。カメラモジュール内に置いた 48 MHz クロックが、システムのグローバルクロックとして使用されている。高速撮像を実現するため、(1)垂直／水平シフトレジスタの駆動クロック周波数をそれぞれ、1 MHz, 48 MHz までクロックアップし、(2) ＣＣＤチップ内で複数の画素を加算し、空間解像度の犠牲を最小限としながら読み出し画素数を減らす方式(ピクセルビニング)を採用した。

[プロセッサユニット]　アナログ信号処理ブロック、Ａ／Ｄコンバータ、フレームメモリ、ＦＰＧＡデバイスｘ２から構成される。ＦＰＧＡのハードウェアロジックは、光計測用ソフトウェアが起動した際、ＰＣからダウンロードされる。入力されたＣＣＤ出力信号は、低域通過フィルタリング、暗レベルにクランプされた後、低ノイズアンプで増幅され、高速Ａ／Ｄコンバータに送り込まれる。デジタル化されたＣＣＤ出

力信号は、ＦＰＧＡを介してフレームメモリに書き込まれる。フレームメモリはＤＲＡＭモジュールで構成し、容量 128 MB を実装した。水平ブランキング期間に、メモリ・リフレッシュが行われるよう設計されている。システムにはイメージデータ用の高速Ａ／Ｄコンバータとは別に、４チャネルＡ／Ｄコンバータが実装されている。これは光計測中に細胞外電極を用いて記録した電場電位や心電計出力波形などをフレームレートでサンプリングし、イメージデータと一緒に保存する目的で使用される。外部トリガのモニタリング、さらにイメージキャプチャに同期したシャッター制御機能を持つ。

[ソフトウェア]　計測用ソフトウェアはウィンドウズベースの MDI/GUI 環境で、実験中のオペレーションが容易に行えることを主眼に開発した。光計測データの獲得、処理、表示、蓄積、解析、印刷と一通りのツール群を装備している。ＰＣにハードウェアが接続されていない状態ではメインメモリにフレームメモリ領域をアロケートし、スタンドアロンＰＣでも光データの解析が可能である。

2) 光計測装置タイプ２

本光計測装置は、サルを測定対象とし、カスタム品の 1.2 インチサイズＣＣＤチップをコアに開発した。(1)ＣＣＤ出力アナログ信号処理を行うヘッドボードと、信号をデジタイズした後、(2)デジタル信号処理を行うプロセスボードを個別開発し、両者を２段重ねとする構成とした。PC/AT コンピュータには、32 ビット PCI インターフェースカードを挿入し、測定データ/制御コマンドの入出力は RS-422 平衡伝送トランシーバ/レシーバを用いて行った（図２）。

[カメラヘッドボード]　ＣＣＤチップの全画素数は 2664(H)x1224(V) であり、Ｈ方向に 24 チャネル分割されている。従って、各チャネルは 111x1224 ピクセルである。各チャネルを並列読み出しすることで高速化が実現される。チップはインターライン転送方式、垂直方向電荷転送は 24 相クロック制御である。96 MHz クロックが源振で、これを４分周した 24 MHz で水平シフトレジスタが駆動される。ここでも、チップ内ピクセルビニング、メモリ内ピクセルビニングを行い、高速イメージング時の空間解像度は 444x200 程度としている。

図２　光計測装置タイプ２の概観(左)と,カスタムＣＣＤセンサ(右)

[プロセスボード]　ＣＣＤチップからの読み出しチャネル数に対応して、24 チャネル独立のフレームメモリを持つ。フレームメモリはＳＤＲＡＭデバイスで構成し、各チャネルに容量 128 MB を実装した。また、メモリ制御、デジタルデータ処理、インターフェース等のロジック回路は、３個のＦＰＧＡデバイスを用いて実現した。

９．結果

1) 光計測装置の性能

光計測装置タイプ１に実装した６種類のイメージングモード I-VI を表１に、光計測装置タイプ２に実装したイメージングモードを表２に示す。

Imaging mode	On-chip binning format	CCD readout pixels after binning	Minimum frame interval T_{min} (msec)	Spatial resolution of images stored in frame memory	Dynamic range of one pixel (bit)	Number of storable frames
I	2 x 2	256 x 246	3.20	256 x 246	8	2131
II	2 x 4	256 x 123	1.80	128 x 123	13	4262
III	2 x 6	256 x 82	1.25	128 x 82	13	6393
IV	2 x 8	256 x 62	1.00	128 x 62	13	8456
V	2 x 10	256 x 50	0.85	128 x 50	13	10485
VI	2 x 12	256 x 41	0.75	128 x 41	13	12787

表１　光計測装置タイプ１のイメージングモード

Imaging mode	On-chip binning format	CCD readout pixels after binning(/CH)	Minimum frame interval T_{min} (msec)	Spatial resolution of images stored in frame memory	Dynamic range of one pixel (bit)	Number of storable frames
I	1 x 6	111 x 1224	2.00	444 x 200	14.58	18000

表２　光計測装置タイプ２のイメージングモード

2) 光計測実験

ラットの１本の“ほおヒゲ”に曲げ刺激を与え、体性感覚野バレル皮質において外因性(１次)シグナルと、内因性(２次)シグナルを記録した。両者のマップを比較した結果を図３に示す。

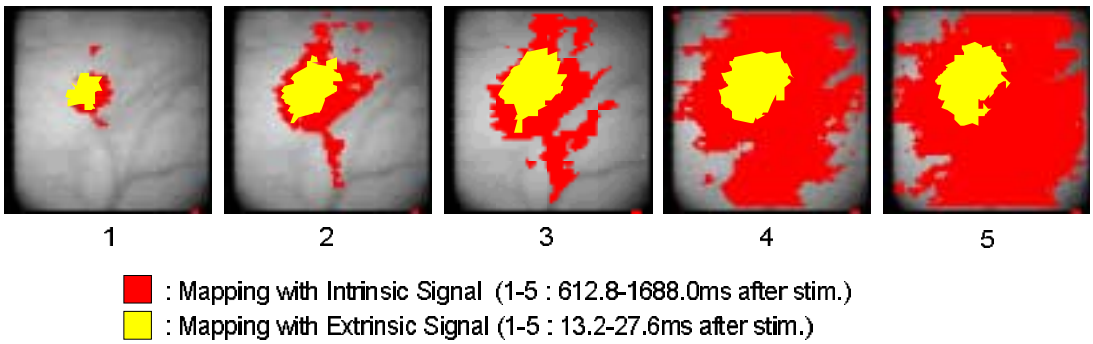

図３　ラットバレル皮質での光計測結果：外因性光シグナルによるマップ(黄色)と、内因性光シグナルによるマップ(赤色)の比較を示す。

10．考察

1) 光計測装置の S/N

ＣＣＤカメラにはいくつかのノイズ源が存在する。ショットノイズ、暗電流ノイズ、ＫＴＣノイズ、増幅器ノイズなどである。この中でもショットノイズは光子の統計的ゆらぎに起因するものであり、光計測においては最も支配的なノイズとなる。我々のシステムの場合(タイプ１)、ビニング処理後、１ピクセルあたり約 75,000 の電子が蓄積されることになる。ショットノイズ成分はこの電子数の平方根と考えてよいから、その割合は約 0.365 % となる。ショットノイズはポアソン分布に従って発生し、画素間で独立な確率現象とみなせるため、N画素を集めることでノイズは １／√N に減らすことができる。隣接２ピクセルでデジタル加算を行えば、ショットノイズ成分は 0.26 % 程度と見積もることができ、開発したシステムにおける実測値と概ね一致する。開発装置では、ＦＰＧＡ内のＤＳＰ回路でデジタル信号処理アルゴリズム(隣接ピクセルを使った３Ｄフィルタリング)を実行させ、時空間解像度を多少犠牲にし

ながら S/N を大きく向上させる工夫も行っている。

2) １次シグナルマップと２次シグナルマップの比較

図３に示すように、応答初期を見れば両者のマップはほぼ一致する。しかしながら、１次シグナルでマップされる神経活動が数百ミリ秒で終わった後、２次シグナルでマップされる代謝活動は数秒間続き、より広範な皮質領域を占めている。この結果は、ｆＭＲＩやＰＥＴで得られる２次シグナルマップから１次シグナルマップ(＝神経活動)を推定する際には十分な注意と考察が必要であり、応答の空間的広がりは、ある種のファクターを乗じて見積もる必要があることを示唆している。

11. 今後の展開

高速光計測法を用いて、１次シグナルと２次シグナルを同時に高精度で記録する手法の基礎的技術に関しては、ほぼ確立されたと言える。しかしながら、信号の S/N に関してみると決して満足できるレベルではない。場合によっては動物の心拍ノイズに埋れてしまう程度の信号しか検出できないこともある。測定結果にアーティファクトを生じさせる外来の振動性ノイズの除去技術、さらには、より低ノイズ、高感度半導体素子の使用による電気的ノイズの低減などは、今後に残された課題と言えよう。
また、光計測法というツールを用いて、１次シグナルと２次シグナルの関係を調べる研究、２次シグナルの発生機序を調べる研究は、まだまだ始まったばかりである。新しい情報や知見が日々、蓄積されている状況である。計測技術の開発と計測実験結果の解析は、研究を進める両輪であるから、今後は開発した装置を用いて多くの実験を行い、本質に迫る計測を行うためのアイデアを、計測技術にフィードバックしていく必要がある。

その一例を挙げれば、以下の通りである。内因性光シグナル計測では、測定光波長により異なる機能マップが得られるが、現状では予め数種の帯域フィルタを準備しておき、これを差し替えて計測を行っている。同時に多波長分光画像を得たいという要求は強く、レンズアレイと干渉光学系、多ピクセル撮像素子を用いた分光画像計測システムの可能性について検討を始めている。

13. 研究業績

13-1. 原著論文

[1] I.Takashima, M.Ichikawa and T.Iijima : High-speed CCD imaging system for monitoring neural activity *in vivo* and *in vitro*, using a voltage-sensitive dye, Journal of Neuroscience Methods, 91, pp.147-159 (1999)

[2] I.Takashima, R.Kajiwara, K.Murano, T.Iijima, Y.Morinaka and H.Komobuchi : High-speed high-resolution epifluorescence imaging system using CCD sensor

and digital storage, for neurobiological research, Proceedings of SPIE (2000, in press)

[3] R.Kajiwara, I.Takashima, K.Murano, Y.Mimura and T.Iijima : High-speed videography system using a pair of imagers for biological applications, Proceedings of SPIE (2000, in press)

13-2. 総説など：なし

13-3. 国際学会発表

[1] I.Takashima, M.Shinoda and T.Iijima : Long-term monitoring of neural activity using high-speed optical imaging system equipped with consumer-grade CCD device, Society for Neuroscience (1998)

[2] T.Iijima, I.Takashima, M.Inase, R.Kajiwara, M.Shinoda, T.Takahashi, K.Tsukada, H.Hirose and K.Niisato : Real-time optical imaging provides “dynamic map” of brain activity, The 5th International conference on neural information processing (ICONIP’98), (1998, Kitakyusyu)

[3] I.Takashima and T.Iijima : Optical imaging of neuronal activity and coupled metabolic activity in rat barrel cortex, Society for Neuroscience (1996)

13-4. 国内学会発表

[1] 高島一郎，篠田真由美，飯島敏夫：高速ＣＣＤイメージングシステムによる神経活動の長時間光学測定，第 21 回日本神経科学大会 (1998，東京)

[2] 高島一郎，飯島敏夫：光計測法による、ラットのバレル皮質での神経活動と代謝活動のイメージング，第 19 回日本神経科学大会 (1996，神戸)

13-5. 新聞など：なし

13-6. 特許

[1] 梶原利一、高島一郎、飯島敏夫：画像信号処理システム、特願 2000-118378（平成 12 年 4 月 19 日）

14. High-speed Optical Imaging Method

15. Electrotechnical Laboratory

16. Ichiro Takashima (Supermolecular Science Division, Electrotechnical Lab.)

17. Toshio Iijima (Supermolecular Science Division, Electrotechnical Lab.)
Riichi Kajiwara (Supermolecular Science Division, Electrotechnical Lab.)
Hiroyoshi Komobuchi (Advanced Technology Research Lab., Matsushita Electric Industrial Co., Ltd.)

Yasuhiro Morinaka, (Advanced Technology Research Lab., Matsushita Electric Industrial Co., Ltd.)

18. 1996 - 2000

19. Abstract

The high-speed optical imaging method has been studied for monitoring neural and metabolic activities in the brain. During the research period, an optical imaging system was newly developed, which has the following specifications: (1) A CCD (Charge Coupled Device) is utilized as an imager. (2) The shot noise S/N level is more than 68dB. (3) The frame rate exceeds 1000 fps. (4) An optical apparatus designed to be nearly uniform illumination over the imager, and (5) a software package of window-based GUI environment are incorporated.

Utilizing our optical imaging system, two kinds of optical signals resulting from brain activity were successfully monitored, i.e. (A) extrinsic optical signals (primary signals) coming from a voltage-sensitive dye and (B) intrinsic optical signals (secondary signals) due to changes in functional perfusion. The system enabled us to monitor both neural and metabolic activities from the same cortical area of interest in the experiments, which provided fruitful information to understand the relationship between the primary and the secondary signals.

ELSEVIER

Journal of Neuroscience Methods 91 (1999) 147–159

JOURNAL OF NEUROSCIENCE METHODS

www.elsevier.com/locate/jneumeth

High-speed CCD imaging system for monitoring neural activity in vivo and in vitro, using a voltage-sensitive dye

Ichiro Takashima, Michinori Ichikawa, Toshio Iijima *

Supermolecular Science Division, Electrotechnical Laboratory, 1-1-4 Umezono, Tsukuba, Ibaraki 305-8568, Japan

Received 1 March 1999; received in revised form 15 June 1999; accepted 23 June 1999

Abstract

We have designed and constructed a high-speed CCD imaging system for optically detecting neural activity from preparations stained externally with a voltage-sensitive dye, and have used this system to image evoked and epileptiform neural activity in the rat somatosensory cortex. The imaging system uses a commercially available 1/3-in. CCD chip, and it can continuously capture images for more than 8 s, at 1000 frames/s, with a spatial resolution of 128×62 pixels. The spatial/temporal resolution of the CCD sensor is variable by changing the geometry of on-chip binning pixels, which can be controlled by a PC/AT computer. Dye bleaching correction was not necessary for long-term imaging of epileptiform neural events, since the sensitivity of the CCD sensor was increased by combining the signal from adjacent pixels.

Keywords: Optical imaging; CCD; Voltage-sensitive dye; Epileptiform discharge; Somatosensory cortex

1. Introduction

Optical imaging of neural activity with a voltage-sensitive dye is a powerful technique to investigate the dynamic functions of the brain, and it has become a popular method in the neuroscience field. Early efforts at multiple-site optical recording utilized 10×10- or 12×12-element photodiode matrix arrays (Grinvald et al., 1981; Salzberg et al., 1983; Cohen and Lesher, 1986), and neural activity was successfully monitored (Orbach and Cohen, 1983; Grinvald et al., 1984; Orbach et al., 1985; Kauer et al., 1987; London et al., 1989; Cinelli and Salzberg, 1990, 1992). Since then, higher spatial/temporal resolution and better signal-to-noise ratios have been achieved using 16×16-, 22×22-, 24×24- and 34×34-element photodiode arrays (Iijima et al., 1992; Nakashima et al., 1992; Falk et al., 1993; Hirota et al., 1995). While photodiode array sensors have high temporal resolution because of their parallel readout method, their spatial resolution is intrinsically limited.

In contrast to photodiode arrays, the CCD camera possesses high spatial resolution (several hundred pixels in each dimension) but has poor temporal resolution due to its serial readout scheme. Therefore, the CCD cameras have been used for intrinsic signal optical imaging to visualize discrete functional modules of the cortex (Frostig et al., 1990; Ts'o et al., 1990). Because of a slow time course of intrinsic signals (rise time > 1 s), commercially available CCD cameras (capturing several frames/s) can be used for intrinsic signal imaging. Some groups, however, have increased the speed of CCD cameras by utilizing spatial integration on the CCD chip, and have used them for fura-2 fluorescence imaging and voltage-sensitive dye recording (Lasser-Ross et al., 1991; Cabo et al., 1994; Kleinfeld et al., 1994; Gogan et al., 1995; Kogan et al., 1995). Their CCDs operated at reduced spatial resolution in exchange for higher frame rate. For example, Lasser-Ross et al. (1991) have run a scientific-grade cooled CCD camera at 100 frames/s after binning to 18×18 pixels, or at 40 frames/s after binning to 50×50 pixels. More recently, a unique CCD camera with a subregion imaging technique has been introduced (Potter et al., 1997). The system used 64×64-pixel array CCD chip and allowed users to select any arbitrary set of pixels of

* Corresponding author. Tel.: +81-298-545556; fax: +81-298-545559.

E-mail address: iijima@etl.go.jp (T. Iijima)

0165-0270/99/$ - see front matter
PII: S0165-0270(99)00093-X

interest. It produced movies of selected 1000 pixels at ~500 frames/s, but ~120 frames/s for full-frame imaging (with an integration time equal to the frame readout time). Thus, none of these CCD systems had millisecond time resolution for tracing the dynamics of neural action potentials, covering a wide cortical area with sufficient spatial resolution.

In our laboratory, a MOS-based monolithic array camera (128 × 128 elements) having temporal resolution of 0.6 ms has been developed (Ichikawa et al., 1993), and it has successfully imaged neuronal activity in rat hippocampal (Barish et al., 1996) and entorhinal–hippocampal slices (Iijima et al., 1996). The system combines the temporal resolution of photodiode arrays and the spatial resolution of CCD devices. However, it required signal averaging in some experimental conditions, and it was not suitable for imaging more than 2 s of activity, because of its small capacity frame memory (16 MB) and because of dye-bleaching drift beyond its dynamic range. To circumvent these limitations, we have developed a CCD imaging system having spatial/temporal resolution and signal-to-noise ratio comparable to the previous solid-state camera. We have incorporated well-defined ideas, such as on-chip binning and computer-controlled spatial/temporal resolution changes, into the new imaging system, and have successfully used the system for imaging seconds–long periods of neural activity.

This paper describes the design of the high-speed CCD imaging system, and presents some experimental data obtained with the system.

2. Materials and methods

2.1. Construction of the system

The CCD imaging system is composed of a camera module and a processor unit as shown in Fig. 1. The small (5 × 5 × 9 cm) light weight (225 g) camera module is attached to an optical apparatus with a C mount adapter. The processor unit is controlled by a PC/AT computer with an interface board plugged in a 16-bit ISA bus slot (not shown). The interface board, used for sending control-commands and transferring data between the imaging system and the computer, was newly developed for the imaging system. The camera module and the processor unit are connected with a cable including three coaxial and eight single lines; the cable is 7 mm in diameter and can be up to 2 m long. A highly stabilized DC power is necessary to improve the signal-to-noise ratio of the imaging system.

2.1.1. Camera module

The imaging sensor used for our system is a consumer-grade 1/3-in. CCD chip (MN3716MAE, Panasonic, Osaka, Japan). The chip has been manufactured for home-use camcorders and is easy to obtain. The chip has 512 × 492 pixels, adopting an interline-transfer organization. The CCD chip employs 4-phase clocking as a vertical charge shift operation, and a V-driver chip (MN3112SA, Panasonic) for this CCD chip is provided. The most widely used CCDs in video-rate cameras are of the interline design. Because of its low optical collection efficiency and poor quantum efficiency, the interline-transfer device has been rarely used for scientific imaging. However, the advantages of this architecture is that it is inexpensive to produce, and that it allows continuous light exposure even during the period of charge transfer since the charge transfer pathways are masked and isolated from the photosensitive area. After the termination of an exposure, the accumulated photoelectrons are simultaneously transported from the photosensitive area to the charge transfer registers, and the next exposure starts instantly. Therefore, the data of every pixel in one frame are recorded simultaneously, though the charges are serially read out in the next exposure period. Hardware logic circuits consisting of a DAC controller, a command decoder and of a timing generator were implemented in an FPGA (Field Programmable Gate Array) device (XC4003E, Xilinx, San Jose, CA). This FPGA has a capacity of 5 K gates, and programmed designs are downloaded from a serial configuration PROM when power is applied to the device. A 48 MHz clock pulse was used as a global clock in the FPGA.

Electrons generated in an array of photodiodes in the CCD chip are successively transferred to a readout amplifier via vertical and horizontal shift registers in the chip. The timing generator block in the FPGA generates drive pulses for vertical ($V_1 - V_4$, CH_1–CH_2) and horizontal (H_1–H_2) shift operations. A pre-charge pulse (RS) is also generated to control the pre-charge gate of the CCD chip. High-speed CCD readout was achieved by increasing the on-chip clock frequency, and by reducing the number of readout pixels with an on-chip binning method. The drive clocks of the vertical and the horizontal shift registers were increased up to 1 and 48 MHz, respectively. The drive pulse sequences are designed to combine individual photodiodes into superpixels on the horizontal shift register and on the output node.

In our implementation, the command decoder block in the FPGA receives a mode-command and a frame_rate-command from the processor unit. The mode-command changes its imaging mode; Table 1 summarizes the six imaging modes implemented and their specifications. The imaging modes differ in the geometry of binning pixels. When the imaging mode changes, the timing generator block dynamically changes the drive pulse sequences for the specified binning format. The readout rate of the CCD chip is always 24 MHz, since

the horizontal shift register is driven at 48 MHz and two pixels are binned horizontally in every imaging mode. The DAC controller block adjusts output voltages of a Trim-DAC device (DAC-8800, Analog Devices, Norwood, MA) when the mode-command is accepted. The Trim-DAC device supplies several bias voltages to the CCD chip (e.g. substrate voltage, P-well voltage, output amplifier drain supply voltage, and output gate bias voltage), and which are readjusted to optimum values when the on-chip binning format is changed. Once the imaging mode is selected, the number of readout pixels is fixed, and the minimum frame interval T_{min} is determined as shown in Table 1. The frame_rate command changes the frame interval by using the timing generator block function. An arbitrary frame interval ($\geq T_{min}$) can be set in 25 μs increments.

The frame interval and the light-integration time are equal for the interline-transfer CCD. The frame interval determines the charge accumulation period of the CCD chip, and thus the light intensity to which the tissue is exposed. The mode-command and the frame_rate-command can dynamically change the imaging mode and the frame interval, even during the optical imaging experiments.

2.1.2. Processor unit

The processor unit is composed of an analog signal processor block, analog-to-digital converters (ADCs), frame memory (DRAM modules) and two FPGA devices (XC4010, Xilinx). This FPGA has a capacity of 20 K gates, and hardware logic circuits were implemented in the two FPGAs. Each FPGA has a FPGA interface block so that the two devices can communicate and work cooperatively. The two FPGAs are designed to receive their configuration data from the PC/AT computer when the optical imaging software is started.

The processor unit receives a 24 MHz clock pulse, a vertical drive pulse V_d and a CCD output signal from the camera module through the coaxial lines in the cable. The FPGAs use the received 24 MHz pulse as their global clocks, which ensures synchronism between the FPGAs in the camera module and in the processor unit. A clamp pulse generator block in the FPGA receives the V_d pulse which indicates the start of each frame, then generates clamp pulses when the optical black pixels are read out. The optical black pixels which lie by the chip borders are optically overshadowed and can be referred to the dark level. The CCD output signal is low-pass filtered (LPF), and is clamped to the dark level when the clamp pulse is generated. The CCD signal is amplified by a low noise operational amplifier (AD829, Analog Devices), and is then converted to digital signals by the high-speed ADC (AD9042, Analog Devices). A gain controller block selects the gain of the AD829 amplifier, and a DSP block orders the ADC to start A/D conversion by the 24 MHz encode pulse. The ADC-AD9042 is a 12-bit track-and-hold A/D converter which has an ability to provide digital outputs at 41 MSPS (mega-samples/s). An offset bias circuit and another amplifier are placed just before the ADC input for contrast enhancement. Two LPFs are the LC filters designed to work as anti-aliasing filters for the data sampling at 24 MHz, namely the cutoff frequency is tuned around 12 MHz. Therefore little or no cross talk between pixels is estimated at this stage.

The CCD signal is digitized and stored in the frame memory during high-speed image data acquisition. The frame memory consists of four DRAM memory modules (HB56D436BR-6B, Hitachi, Tokyo, Japan), and each module has a memory capacity of 32-Mword × 9-bit (8-bit + 1-bit ECC), allowing for 36-bit word read/write operations with a maximum access time of 60 ns. The DSP block processes the incoming digitized data before entry into the frame memory, and the process differs according to the selected imaging mode. When one of the imaging modes II–VI in Table 1 is selected, horizontally adjacent pairs of pixels are digitally added in the DSP block to make one super-pixel (on-memory binning). Although horizontal spatial resolution decreases from 256 to 128 pixels through this process, the dynamic range of the combined one-pixel becomes 13-bit resolution. The DSP block assigns the upper and the lower 18 bits of the 36-bits data bus for the successive two super-pixels, and writes them to the DRAM at a

Table 1
Specifications of implemented imaging modes

Imaging mode	On-chip binning format	CCD readout pixels after on-chip binning	Minimum frame interval T_{min} (ms)	Spatial resolution after on-memory binning	Dynamic range of one pixel (bit)	Number of storable frames
I	2×2	256×246	3.20	256×246	8	2131
II	2×4	256×123	1.80	128×123	13	4262
III	2×6	256×82	1.25	128×82	13	6393
IV	2×8	256×62	1.00	128×62	13	8456
V	2×10	256×50	0.85	128×50	13	10 485
VI	2×12	256×41	0.75	128×41	13	12 787

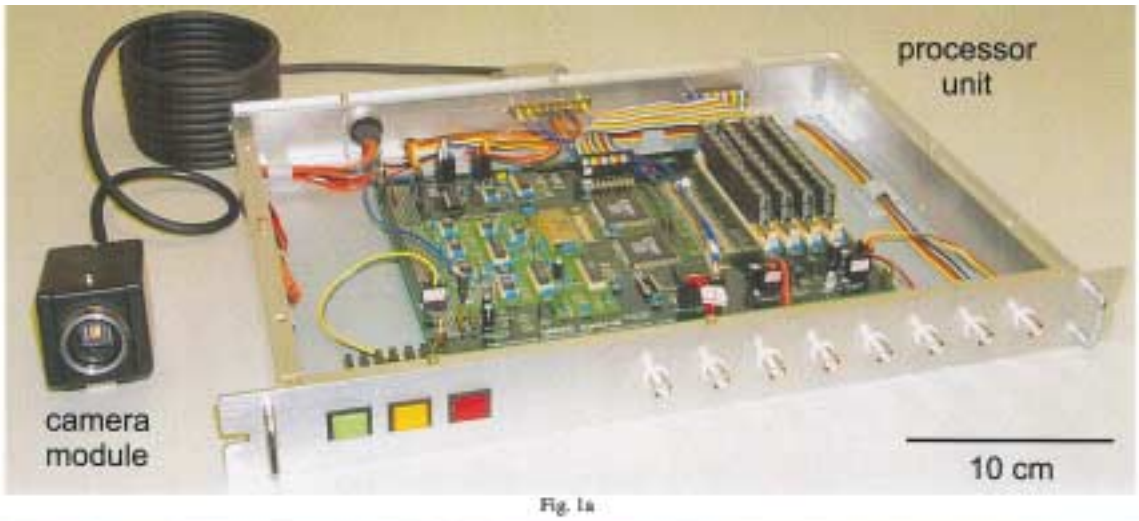

Fig. 1a

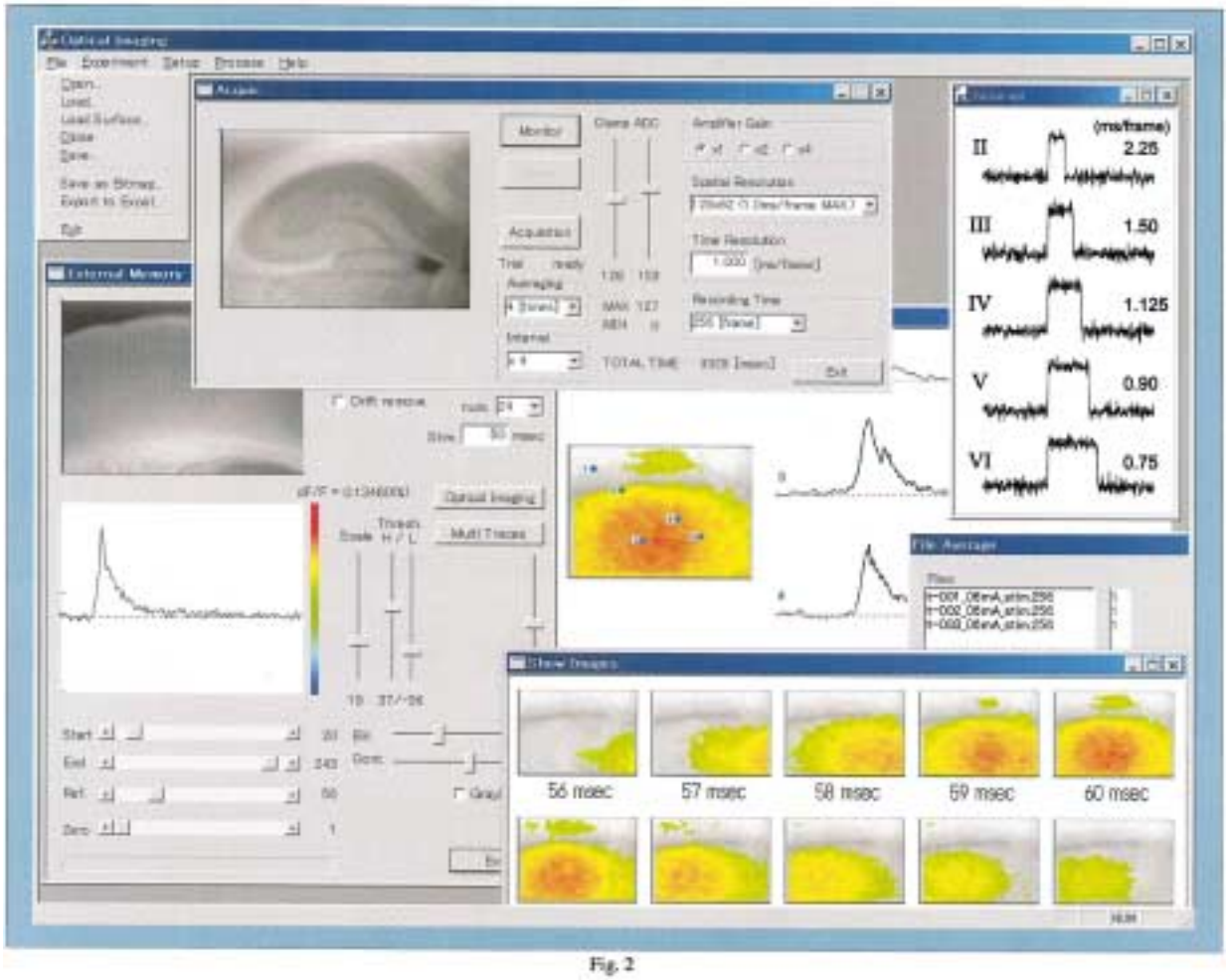

Fig. 2

Fig. 1A and Fig. 2.

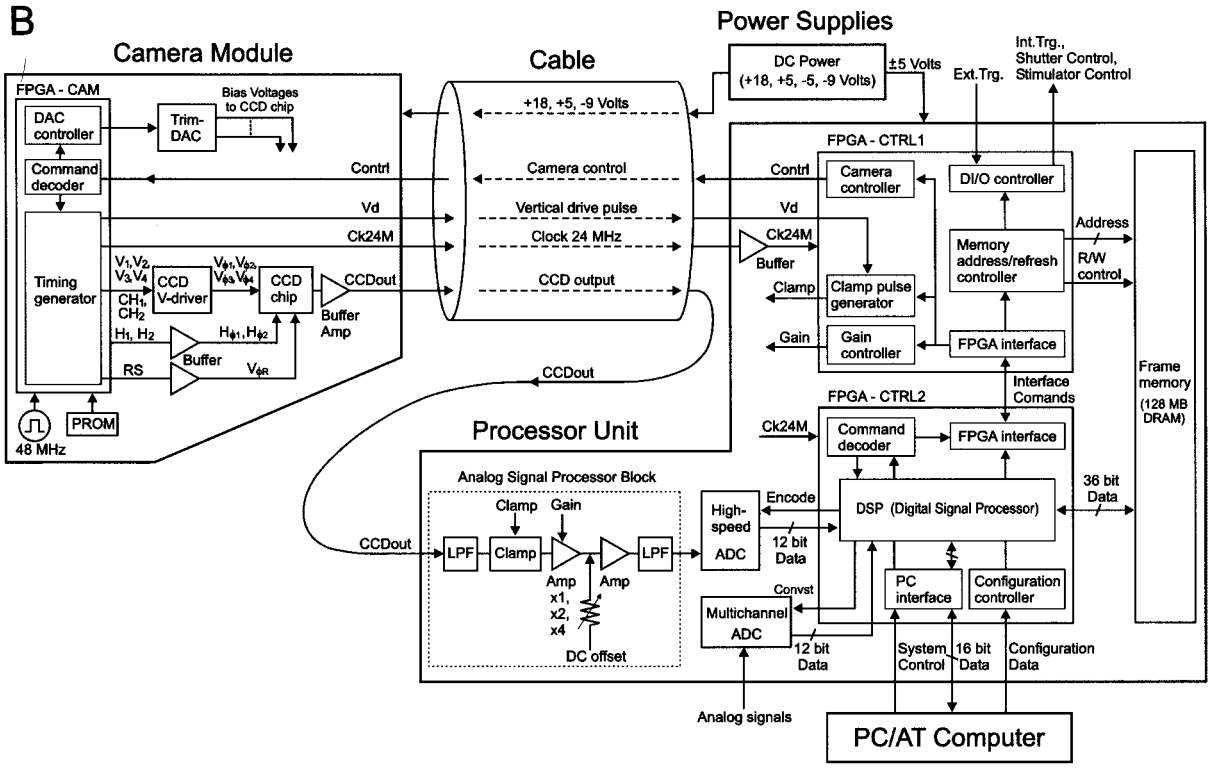

Fig. 1. An overview of the CCD imaging system. A, an outlook of the camera module and the processor unit; B, a block diagram of the system. See text for details.

time. The speed of data flow is consequently transformed from 24 MHz/12-bits to 6 MHz/36-bits by the DSP block. When the imaging mode I is selected, the DSP block ignores the less significant 4-bits of the 12-bit ADC-output, and takes 8-bits from the most significant bit. Subsequently, four 8-bit data blocks from four pixels are concatenated as 32-bit data, and they are written to the DRAM with one write-sequence. The dynamic range of a single pixel is reduced to 8-bit resolution through this process, though horizontal resolution remains 256 pixels. Since the DSP block executes the memory-write operation every fourth pixel, the rate of data flow is also reduced from 24 to 6 MHz in this imaging mode. The spatial resolution (with the dynamic range of one-pixel) of images acquired in each imaging mode is summarized in Table 1. The number of storable frames is also calculated, assuming that the entire frame memory is filled. In the practical experiments, the imaging modes II–VI are utilized for high-speed optical recordings, while the imaging mode I is used for taking clear morphological images on which the optically detected neural activity is mapped. A memory address/refresh controller block manages the frame memory and enables such flexible memory utilization. It is designed to refresh DRAM in the horizontal blanking period, in which the pixel readout is paused because of the parallel shift operation in the CCD chip.

The multichannel ADC (AD7864, Analog Devices) is equipped to digitize analog signals recorded during optical imaging, such as field potentials and electrocardiogram signals. The ADC-AD7864 is a four-channel simultaneous sampling 12-bit A/D converter, and its maximum throughput is 500 kSPS (kilosamples/s). The DSP block sends conversion pulses to the ADC in the horizontal blanking periods and the digitized analog

Fig. 2. A software package developed for optical imaging. The acquisition window (upper middle) shows the current settings of the imaging system. The image of the preparation is redrawn every 1 s in the monitor-mode, which enables easy positioning of electrodes. In the analysis window (lower left) and the signal window (center), the time course of the optical signal is traced when a pixel is specified by mouse clicking. Using the color code adjusted in the analysis window, the image window (lower right) displays a sequence of images at even intervals between the start and the end frames. File averaging is processed in the extreme right window. The upper right window shows the optical signals recorded in different imaging modes, and the result is discussed in Section 3.3.

signals are incorporated with the imaging data and stored in frame memory.

A PC interface block receives different kinds of system control commands. The mode-command and the frame_rate command stated above are relayed to the camera module via a camera controller block. A parameter-command indicates imaging parameters, such as the number of frames to be acquired, the trigger mode, the number of trials to be averaged, the interval between trials, the starting address of the memory, and so on. An acquisition-command initiates the image acquisition in the internal trigger mode; a DI/O controller block senses the external trigger pulse in the external trigger mode, and which enables frame acquisition synchronized with the electrocardiogram for in vivo applications. The above-mentioned DSP block also processes an average-command, a differential-command and a filter-command. The average-command directs the DSP block to add images stored in frame memory during trial-averaging acquisition. A maximum of 32 trials may be averaged, since one pixel has 18-bits of memory capacity, while data is acquired at 13-bit resolution ($2^{(18-13)} = 32$). When the differential-command is accepted, the DSP block subtracts a reference image from the images stored in frame memory. Because of hardware simplicity, the image subtraction is carried out digitally in the system, though it is preferable to subtract in the analog domain (Ichikawa et al., 1993). The DSP block does spatial/temporal filtering of memory data when the filter-command is issued. There is a load/save-command for downloading or uploading image data between the frame memory and the computer.

2.2. Software

A software package was developed in a window-based MDI/GUI (Multi-Document/Graphical User Interface) environment (Microsoft Visual C++ 5.0), as shown in Fig. 2. It allows us to send control-commands to the imaging system by using the ISA interface board, and it also offers software tools for collecting, processing, displaying, storing, analyzing and printing the optical data. For data analysis, a part of PC's main memory is allocated to the frame memory so that the software runs without the imaging system hardware. An exporting function is also provided for linking analyzed data to third-party software, for example, images and signal traces can be saved as bitmap and text files, respectively.

2.3. Specimen preparation and staining

2.3.1. In vivo preparation

Male Wistar rats ($\sim$250 g) were anesthetized with intraperitoneal injection of ketamine (80 mg/kg) and xylazine (8.8 mg/kg) followed by atropine sulfate (0.5 mg/kg). A tracheal cannula was inserted and stainless screws were implanted on the skull. The animal was positioned in a stereotaxic head-holder with the screws, and craniotomy (5 × 5 mm) was performed over the left somatosensory cortex. A well of dental acrylic was built around the exposed cortex. After removing the dura matter, the cortical surface was stained with a voltage-sensitive dye RH-795 (Molecular Probes, 0.6 mg/ml) for $\sim$1 h. The dye was then fully washed out and the well was filled with artificial cerebrospinal fluid (ACSF). The composition of ACSF was (in mM): NaCl, 125; KCl, 5; $CaCl_2$, 2; $MgSO_4$, 1.25; NaH_2PO_4, 1.25; $NaHCO_3$, 22; glucose, 10. The animal was artificially respirated after pancuronium bromide injection (3.0 mg/kg i.p.), and anesthesia was maintained by continuous inhalation of Halothane (1.0% in oxygen). Throughout the experiments rectal temperature was maintained at 38°C with a heating pad.

In some optical recordings we used bicuculline because of the following reasons; 1) to compare the evoked optical signal under the normal (control) condition and the enhanced optical signal by bicuculline, and 2) to test the system performance of recording a long-lasting neural event, such as epileptiform activity.

2.3.2. In vitro preparation

Cortical slices were prepared from the somatosensory cortex of male Wistar rats weighing $\sim$250 g. After decapitation under ether anesthesia, the brain was quickly removed and immersed in ice-cold ACSF. A block of somatosensory cortex was removed and sec-

Fig. 3. In vivo optical imaging of evoked neural activity in the barrel cortex before and after the addition of bicuculline to the cortical surface. A, the surface image of the recorded cortical area (4.7 × 3.5 mm). The anatomical whisker barrel map identified after the experiment is superimposed (left, anterior; top, medial). The stimulating electrode was placed outside the view and penetrated obliquely into lower layer VI below the recorded cortical area. Optical imaging was carried out with a spatial resolution of 128 × 62 pixels, and a small rectangle in the figure is the area ($\sim$37 × 56 μm) covered by a single pixel. B, optical signals (lower traces) detected by a pixel (indicated as the rectangle in A), and the field potentials (upper traces) obtained from the same site simultaneously. The optical recordings were carried out before (blue traces) and after (red traces) an application of bicuculline (100 μM), which was dropped over the exposed cortical surface and then washed away 5 min later. The optical signals were acquired for 512 ms at the rate of 1.0 ms/frame. Stimuli were given at 5-s intervals, and eight trials were averaged. C, real-time imaging of neural activity before bicuculline. Neural activity was encoded in pseudocolor (the color code bar in B) and superimposed on the surface image. A fraction of each optical signal, the amplitude of which was below the threshold (background noise) level, was not color coded. The threshold level was determined to be above the fluctuation of the optical signals before the stimulation. The time after stimulation is indicated in each image. D, real-time imaging of the spread of neural activity after bicuculline.

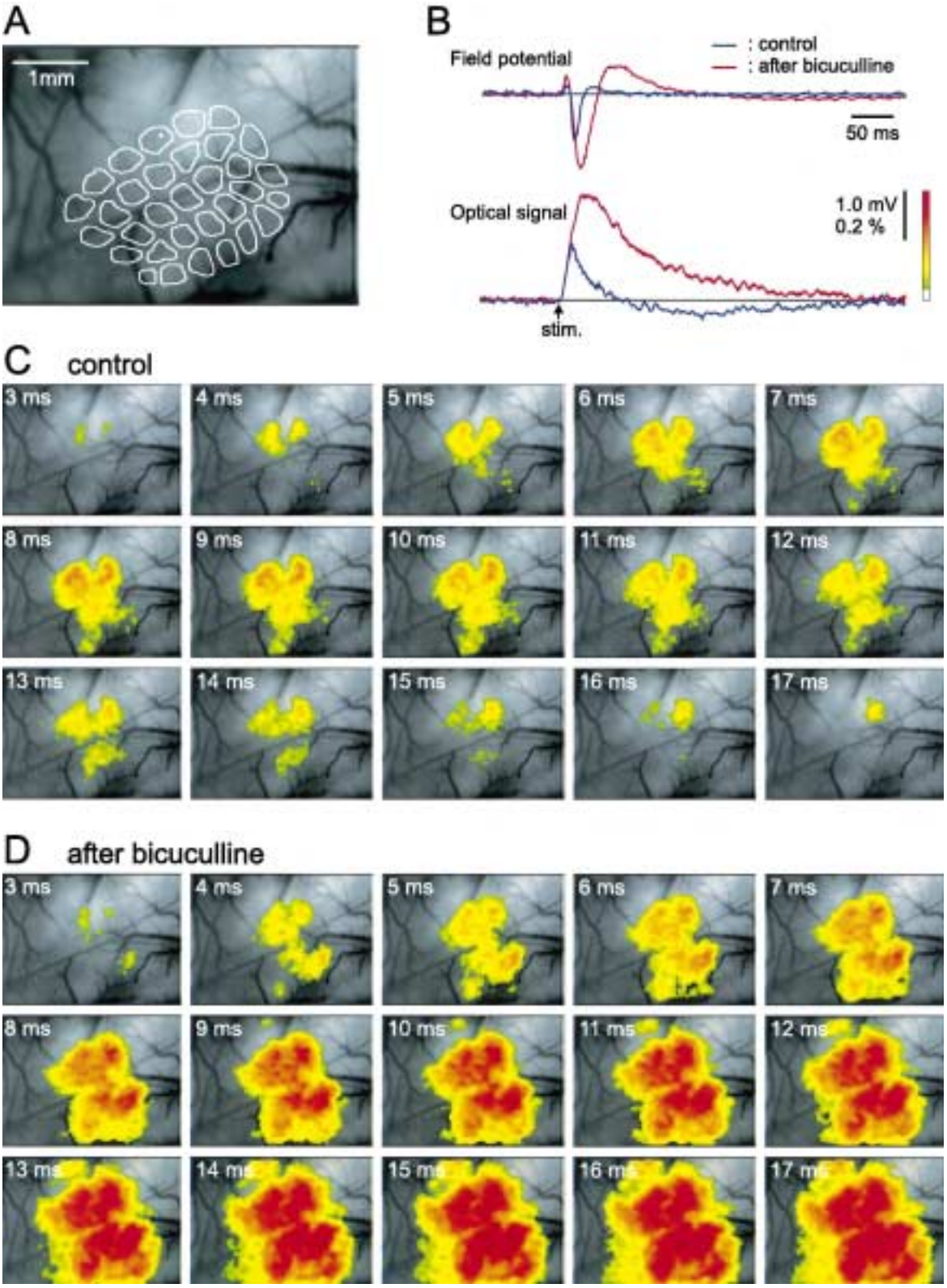
A
1mm
B
Field potential
: control
: after bicuculline
50 ms
Optical signal
1.0 mV
0.2 %
stim.
C control
3 ms
4 ms
5 ms
6 ms
7 ms
8 ms
9 ms
10 ms
11 ms
12 ms
13 ms
14 ms
15 ms
16 ms
17 ms
D after bicuculline
3 ms
4 ms
5 ms
6 ms
7 ms
8 ms
9 ms
10 ms
11 ms
12 ms
13 ms
14 ms
15 ms
16 ms
17 ms

Fig. 3.

tioned in the oblique coronal plane into 400 μm thick slices using a microslicer. The slices were taken at an angle of 50–60° (anterior arc) from the midsagittal plane. The slices then were deposited in ACSF, bubbled with 95% O_2–5% CO_2 at 30°C, and incubated for >1 h before use. The slice was transferred to the imaging/recording chamber and stained with RH-795 (0.5 mg/ml in ACSF) for 3–4 min, followed by >10 min wash in gassed ACSF.

2.4. Electrical stimulation

Electrical stimulation was performed using a bipolar micro-electrode (115 μm tip spacing) made from thin (25 μm diameter) insulated tungsten wires (FHC). For in vivo experiments, the stimulating electrode was inserted into the cortex at an angle of 40–50° from vertical relative to the cortical surface, and the tip of the electrode was positioned in lower layer VI. For in vitro experiments, the electrode was placed at the border of layer VI and the white matter or on the thalamocortical afferent fibers. We selected the stimulus intensity which gave submaximal responses (200 μs in duration, 100–200 μA in intensity).

2.5. Electrical recording

Glass electrodes filled with 0.5 M NaCl (2–8 MΩ) were used to record field potentials. The field potentials were amplified and fed to the processor unit of the imaging system. Digitized field potentials were stored as part of optical imaging data.

2.6. Optical apparatus

The optical apparatus, constructed in our laboratory, was similar to the tandem type epi-fluorescent microscope of Ratzlaff and Grinvald (1991). We used custom-made $f=50$ mm F/1.2 lenses for both first and second objectives, which results in $1\times$ magnification. Since the CCD chip is 1/3-in. size, the imaged area by this optical apparatus was $\sim 4.7\times 3.5$ mm. The voltage-sensitive dye RH-795 has excitation and emission maxima at 530 and 712 nm, respectively. Illumination from a voltage-stabilized tungsten–halogen lamp filtered at 535 nm (± 20 nm bandpass) was guided to the optical apparatus by an optical fiber. The excitation light was reflected down onto the preparations by a dichroic mirror (half-reflectance wave length of 580 nm) and the fluorescence from the preparation was projected to the CCD sensor through a long-wavelength pass filter (50% transmittance at 600 nm).

2.7. Histology

At the end of in vivo experiments, the animal was sacrificed with an overdose of Nembutal. A block of the brain including recorded cortical area was carefully removed and fixed overnight at 4°C in 4% paraformaldehyde. It was subjected to tangential sectioning (80 μm), and the sections were treated for cytochrome oxidase (CO) reaction (Wong-Riley, 1979). The pattern of vibrissa-related barrels was reconstructed from the 2–3 CO-stained sections of layer IV. The stimulation site was also verified.

After in vitro experiments, slices were fixed in 4% paraformaldehyde for 2 h at room temperature and 30% sucrose in phosphate buffer (pH 7.4), and then cut on a freezing microtome into 70-μm sections. The sections were CO-stained and counter-stained with cresyl violet to identify laminar boundaries.

3. Results and discussion

The high-speed CCD imaging system was used to image neural activity in the rat somatosensory cortex. Optical imaging as shown below was performed with spatial resolution of 128×62 pixels (using the imaging mode IV in Table 1), and neural activity was mapped onto a surface image acquired at 256×246 pixels (using the imaging mode I in Table 1). We frequently used bicuculline in the experiments to enlarge the optical signal and to induce epileptiform discharge.

3.1. In vivo optical imaging

Fig. 3 shows the in vivo optical imaging of neural activity in the somatosensory cortex evoked by cortical stimulation. The recorded cortical area was positioned to cover the posteromedial barrel subfield, as shown in Fig. 3(A). Fig. 3(B) shows the optical signals detected by a single pixel before and after an application of bicuculline. Since brain movement artifacts were small, the heartbeat subtraction procedure was not required, and the heartbeat noise disappeared after averaging of eight trials. The optical signals were correlated with field potentials recorded simultaneously from the same site. The fractional change ($\Delta F/F$) of the control optical signal was $\sim 0.25\%$, while after bicuculline the signal was two times larger in amplitude and was prolonged in duration. Optically detected cortical responses before and after bicuculline are shown in Fig. 3(C–D). Electrical stimulation of lower layer VI initially activated two or three cortical columns. Under control conditions neural activity spread to only neighboring barrels (Fig. 3(C)), while activity extended all over the entire barrel cortex in the presence of bicuculline (Fig. 3(D)).

Fig. 4 shows in vivo optical imaging of epileptiform discharge in the somatosensory cortex. The recorded cortical area covered the postero-medial part of the whisker barrel field, as shown in Fig. 4(A). Epileptiform

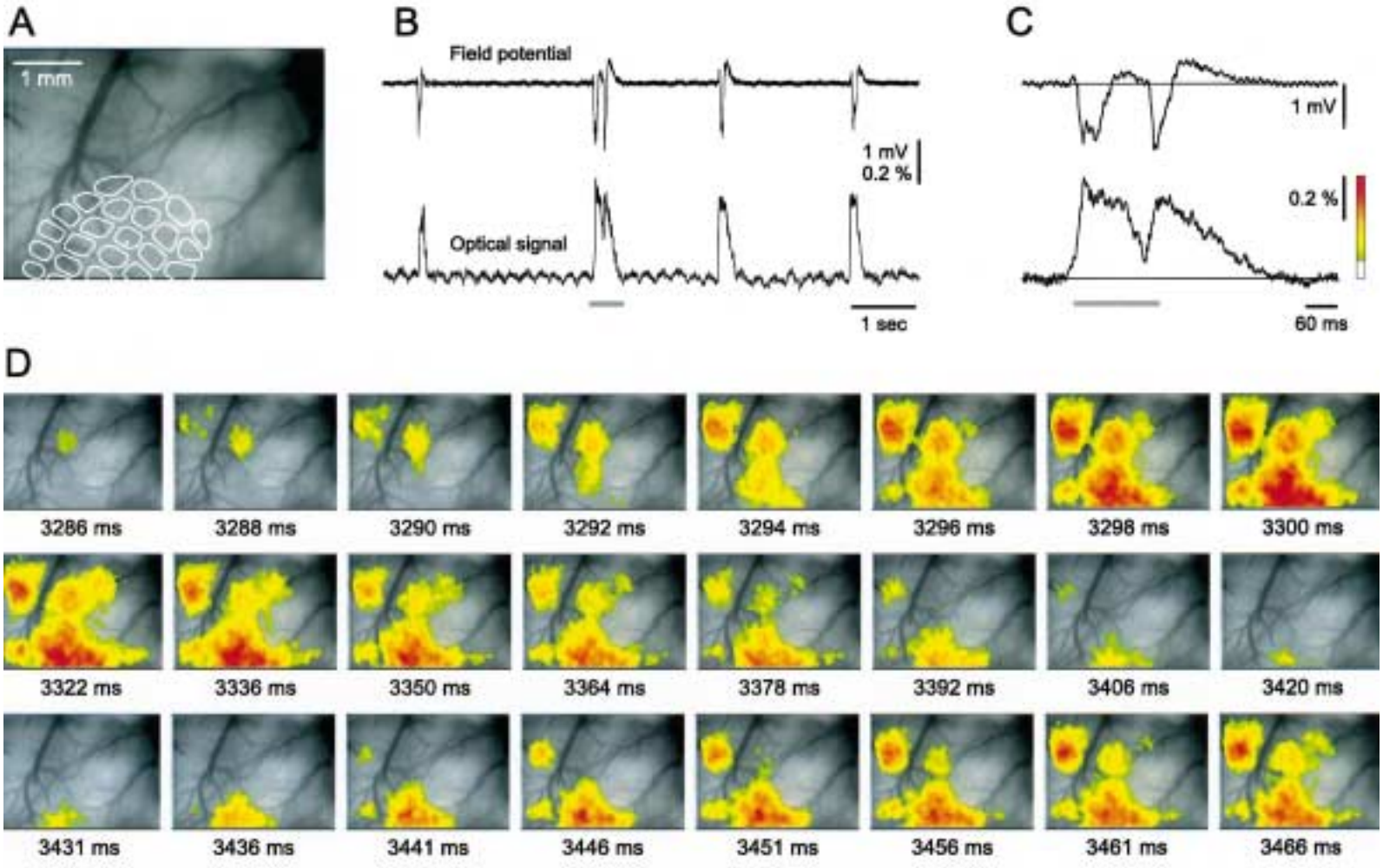

Fig. 4. In vivo optical imaging of epileptiform discharges recorded in the somatosensory cortex. Epileptic events were recorded after dropping bicuculline (500 μM) over the exposed cortex. A, the surface image of the recorded cortical area. The outlines of whisker barrels are superimposed (left, anterior; top, medial). B, an optical signal (lower trace) detected by a pixel (small rectangle in A), and the field potential (upper trace) obtained from the same site simultaneously. Images of 128×62 pixels were acquired for 8192 ms at 1.0 ms/frame. The striking periodic noise of the optical signal was due to the heartbeat. C, magnified traces underlined in B. D, real-time imaging of the spread of epileptiform activity during the period presented in C. The pseudocolor bar in C was used to encode epileptiform activity, and the threshold level was chosen to be above the level of the heartbeat noise. The elapsed time since the beginning of image acquisition is shown below each image. Note that the frames are not selected at regular intervals.

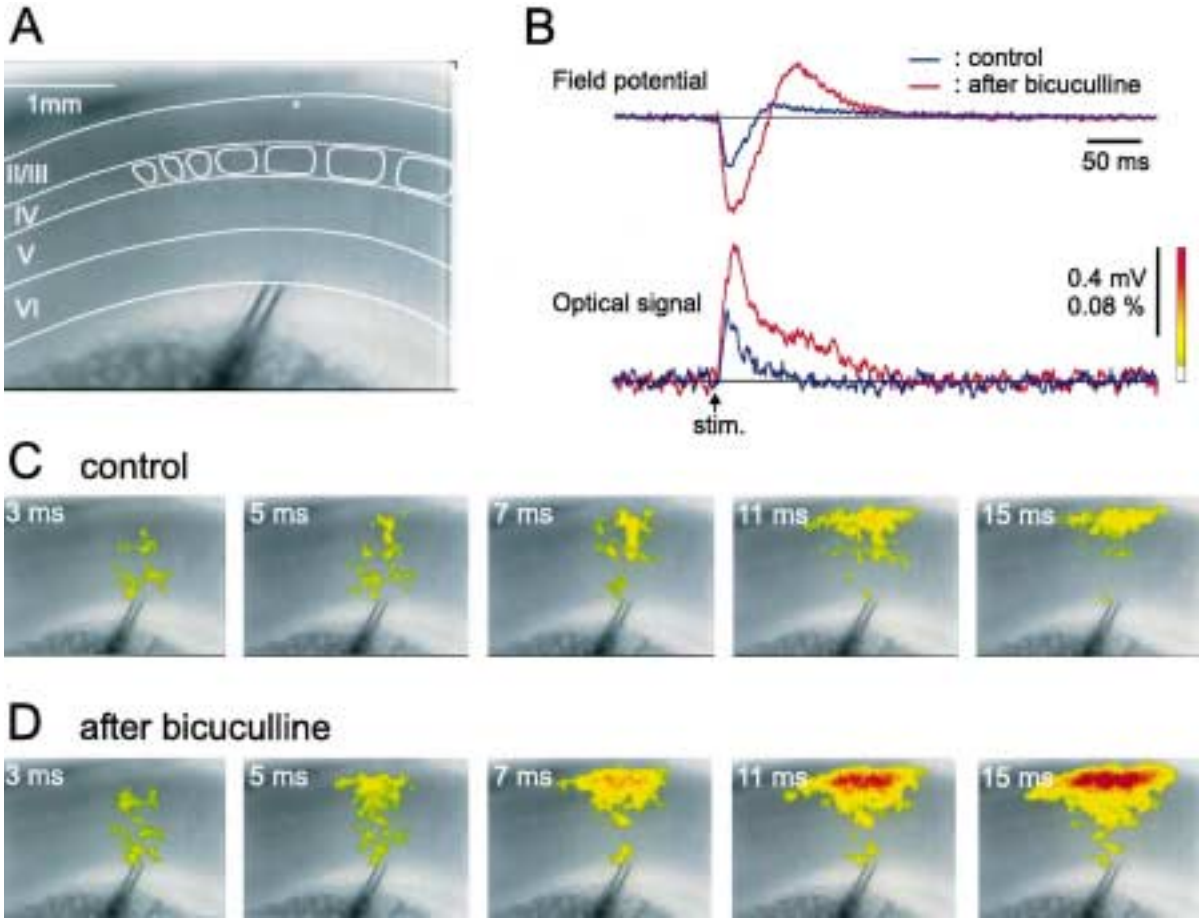

Fig. 5. In vitro optical imaging of evoked neural activity before and after the addition of bicuculline. A, the image of the slice preparation. The outlines of whisker barrels in layer IV and laminar boundaries identified histologically after the experiment, are superimposed. The slice was stimulated at the layer VI-white matter border, and optical signals were acquired for 512 ms at 1.0 ms/image before and after 10 μM bicuculline. B, optical signals (lower traces) recorded by a pixel indicated in A (small rectangle) and the field potentials (upper traces) obtained from the same site simultaneously. Stimuli were given at 5-s intervals, and eight trials were averaged. C, real-time imaging of neural activity before bicuculline; D, after bicuculline. The color code bar used for imaging is shown in B. The time after stimulation is indicated in each image.

discharge was induced by an application of bicuculline. Fig. 4(B) shows the correlation between the optical signal and the field potential. Epileptic events were recorded four times during the recording, and this one-shot optical imaging exhausted the entire capacity of frame memory. The optical signal had a periodic swinging component caused by the heartbeat, and this noise had an amplitude of $\sim 0.04\%$, as compared to the maximum change due to epileptiform discharge of $\sim 0.5\%$. Drift due to dye-bleaching was not evident during the >8 s-long recording. Two successive epileptiform discharges underlined in Fig. 4(B), are shown at an expanded time scale in Fig. 4(C). Fig. 4(D) shows real-time imaging of the epileptifomm activity during this period. The first epileptiform discharge originated from a focus medial to the barrel field and the activity jumped to the anterior area across the large blood vessel. The epileptic activity gradually invaded the barrel field, and spread antero–laterally. The first discharge spontaneously ended, and the second discharge followed immediately. The second epileptiform discharge initiated in the barrel field, and spread posteromedially, retracing the propagation of the first discharge.

3.2. In vitro optical imaging

Fig. 5 shows an in vitro optical imaging of evoked neural activity in the somatosensory cortical slice. Several whisker barrels were included in the slice preparation as shown in Fig. 5(A). The correlation between the field potential recorded in layer II/III and the optical signal detected in a single pixel close to the recording electrode is shown in Fig. 5(B). Bicuculine increased the

peak amplitude of the optical signal approximately twofold. Cortical responses before and after bicuculline were imaged as shown in Fig. 5(C–D). After stimulation, layer IV and lower layer V in which thalamocortical afferent fibers terminate, were activated immediately, and then neural activities spread horizontally in layer II/III. The horizontal spread of activity increased in the presence of bicuculline.

Fig. 6 shows an example of long-time monitoring of neural activity in the somatosensory cortical slice. Images were acquired for 16 384 ms, at a reduced frame rate of 2.0 ms/image. Thalamocortical fibers were stimulated three times during the recording, and bicuculline was dropped to the upper stream of the flowing ACSF between the second and the third stimulation. No responses were recorded to the first and the second stimuli but a response was observed to the third stimulation, as shown in Fig. 6(A). The neural activity evoked by the third stimulus is shown in Fig. 6(B). No dye-bleaching drift was observed, even in optical recordings lasting longer than 16 s.

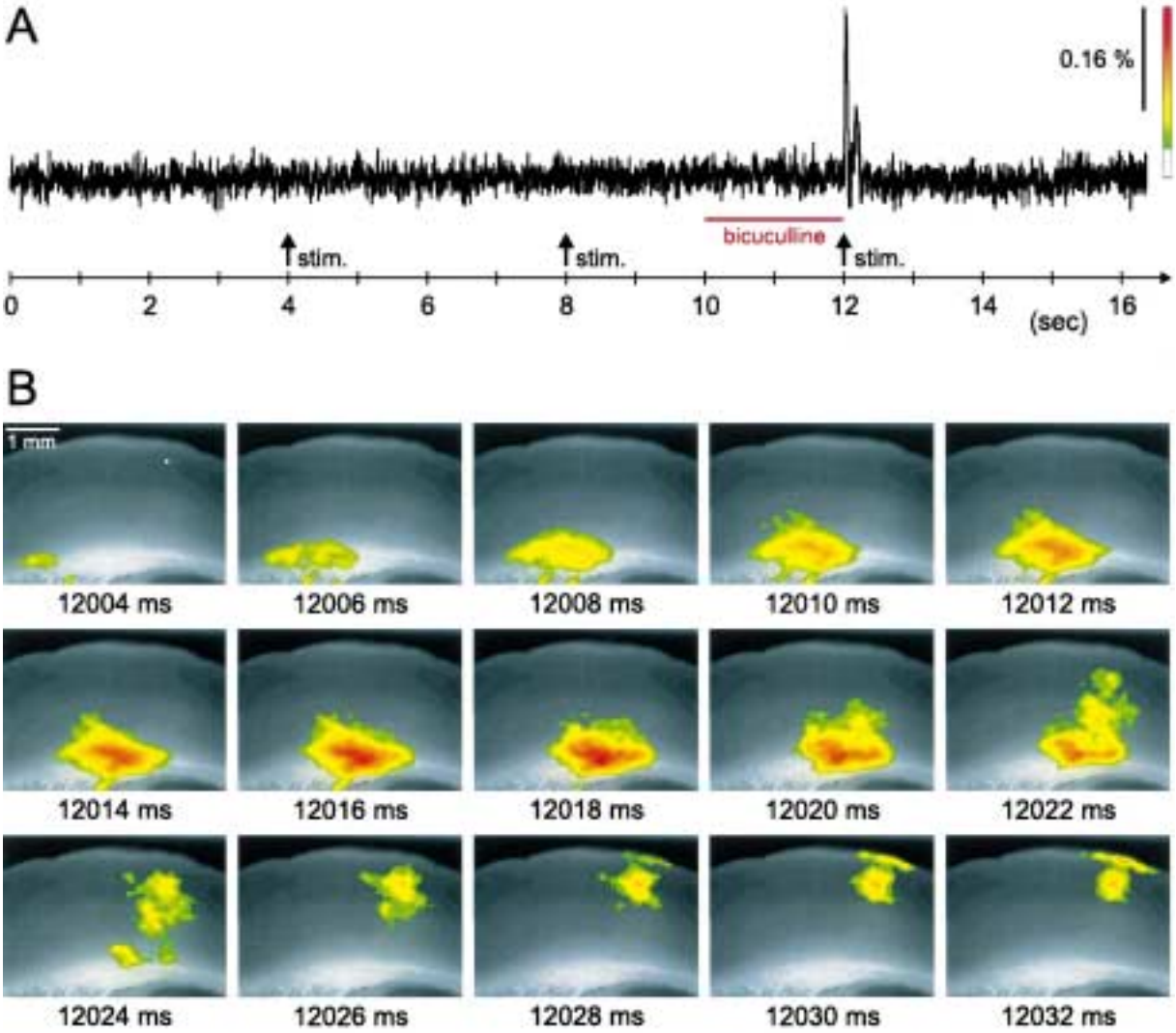

Fig. 6. An example of long-term monitoring of neural activity. The somatosensory cortical slice was placed in the imaging chamber and submerged in flowing ACSF (2.0 ml/min, 25°C). Images of 128×62 pixels were acquired for a period of 16 384 ms at the rate of 2.0 ms/image. Thalamocortical afferent fibers were stimulated at 4, 8 and 12 s since the beginning of image acquisition, and four drops (10 μl/drop) of high concentrated bicuculline (10 mM) were added to the upper stream of the flowing ACSF between 10 and 12 s. The stimulating electrode was outside of the view. A, an optical signal recorded by a single pixel (small rectangle in the first frame in B). B, real-time imaging of neural activity in response to the third stimulation. The elapsed recording time is shown below each image. ACSF was flowing from left to right in the images.

3.3. Signal-to-noise considerations

A commercially available CCD chip was used in our imaging system, and the chip worked with high-speed clocks and voltage-supplies over specifications that the manufacturer guaranteed. We were worried that the life span of the CCD chip might be short, however the system has been working without any trouble for six months until now. It seems that the chips are tolerant and will stand our usage. After screening of four CCD chips in the optical recording experiments, two chips showed good performance, but the rest were middling. The difference of production lots seems to be a possible reason for the uneven quality.

There are several noise sources in CCD cameras, for example shot noise, dark current noise, KTC noise, amplifier noise, and so on. And shot noise, which results from statistical variations in the photon flux, is the most influential noise for optical recording. According to calculations, $\sim 75\,000$ electrons/super pixel are collected in the CCD chip after on-chip binning. Because shot noise is the square root of the photonic signals in electrons, it is estimated to be $\sim 0.365\%$ of the whole accumulated electrons when the chip is illuminated to 100% saturation. Shot noise occurs according to the Poisson process, and it can be approximated with a Gaussian distribution when a large number of photons arrive to the CCD chip (Davenport and Root, 1958). Assuming that shot noise is statistically independent between pixels, it can be reduced to $1/\sqrt{N}$ by gathering N pixels based on the central-limit theorem. We digitally added horizontally adjacent pairs of pixels for the imaging mode II–VI, which resulted in reduced a shot noise of $\sim 0.26\%$. However, it is still not a satisfactory noise level for one-shot imaging of neural activity. Therefore, we implemented the digital filters as a part of the DSP function, which highly improved the signal-to-noise ratio at the slight sacrifice of spatial/temporal resolution. Let $P(m, x, y)$ denote the digitized pixel intensity at a coordinate (x, y) of m-th frame, and $P_F(m, x, y)$ be the filtered data. The 3-dimensional mask filter we have used for one-shot imaging is

$$P_F(m,x,y) = \sum_{\Delta m=-1}^{1}\sum_{\Delta x=-1}^{1}\sum_{\Delta y=-1}^{1} c(\Delta m,\Delta x,\Delta y).\; P(m+\Delta m, x+\Delta x, y+\Delta y) \Big/ \sum_{\Delta m=-1}^{1}\sum_{\Delta x=-1}^{1}\sum_{\Delta y=-1}^{1} c(\Delta m,\Delta x,\Delta y)$$

where

$$\begin{aligned}
&c(-1,-1,-1)=0,\ c(-1,-1,1)=0,\ c(-1,1,-1)=0,\ c(-1,1,1)=0,\\
&c(1,-1,1)=0,\ c(1,1,-1)=0,\ c(1,1,1)=0,\ c(-1,-1,0)=1,\ c(-1,0,-1)=1,\ c(-1,0,1)=1,\\
&c(-1,1,0)=1,\ c(0,-1,-1)=1,\ c(0,-1,1)=1,\ c(0,1,-1)=1,\ c(0,1,1)=1,\ c(1,-1,0)=1,\\
&c(1,0,-1)=1,\ c(1,0,1)=1,\ c(1,1,0)=1,\ c(-1,0,0)=2,\ c(0,-1,0)=2,\ c(0,0,-1)=2,\\
&c(0,0,1)=2,\ c(0,1,0)=2,\ c(1,0,0)=2,\ c(0,0,0)=4
\end{aligned}$$

are the weight coefficients. Two runs of this filtering decreased shot noise by $\sim 0.04\%$. The values of the weight coefficients were changed according to the number of trial averaging.

The optical signals in response to a step change in light intensity were recorded in different imaging modes. The results are laid together in the upper right window in Fig. 2 when an electric current to a light emitting diode was changed for 100 ms. No significant difference in signal-to-noise ratio was observed when the imaging mode was changed. Because the frame rate in each imaging mode was determined so as to be in inverse proportion to the number of on-chip binning pixels, the result again suggests that shot noise is the most dominant in optical imaging. Therefore, a selection of imaging modes just depends on the significance of either spatial or temporal resolution in particular experiments for the users.

4. Conclusion and future improvements

A high-speed CCD imaging system newly developed for optical imaging and examples of its application have been described in this report. The new system has a number of important features, i.e. (1) An inexpensive consumer-grade CCD chip is used. The camera module and the processor unit are very compact to handle and easy to combine with the electrophysiological setups. (2) A high-speed CCD readout circuit was implemented. Images of 128×62 pixels may be sampled and stored at 1.0 ms/image. (3) The hardware logic circuits were designed by using reconfigurable FPGA devices. This enables us to tune the hardware to meet the needs of particular experiments. (4) Spatial and temporal resolution can be dynamically changed by computer control. It is possible in the same experiment to obtain morphological images with high spatial resolution and acquire activity images with high temporal resolution. (5) The signal-to-noise ratio of the camera is improved up to 65 dB, which enabled one-shot imaging of neural activity. (6) A large capacity of frame memory makes

practical continuous optical imaging for more than 8 s. (7) In general, dye-bleaching correction has not been necessary for long-time imaging. The intensity of illumination used for imaging was about one third of that required for the MOS-based solid-state camera developed in our laboratory (Ichikawa et al., 1993). Because of on-chip integration, when the frame rate is decreased to 4·0 ms/image, the illumination intensity necessary to form an image also decreases. Therefore, we expect to be able to perform optical imaging for a period of 32 s without dye-bleaching drifts.

We have successfully imaged epileptic activity induced by bicuculline, however the system's performance for imaging normal spontaneous activity has to be evaluated in further experiments. We are also planning to increase the capacity of frame memory, which will allow us much longer periods of optical imaging with high temporal resolution. After that, we will decrease the time to transfer imaging data to the PC by implementing a high-speed 32-bit PCI bus interface board, which enables image data transfer at 132 MB/s.

Acknowledgements

We thank H. Komobuchi for technical advice regarding high-speed CCD read-out; M. Shinoda for help in software programming; M. Matsukawa and R. Kajiwara for their contributions to experiments performed with the imaging system; and M.E. Barish for reading the manuscript and for helpful suggestions. This work was supported by the Agency of Industrial Science and Technology (AIST) of Japan.

References

Barish ME, Ichikawa M, Tominaga T, Matsumoto G, lijima T. Enhanced fast synaptic transmission and a delayed depolarization induced by transient potassium current blockade in rat hippocampal slice as studied by optical recording. J Neurosci 1996;16:5672–87.

Cabo C, Pertsov AM, Baxter WT, Davidenko JM, Gray RA, Jalife J. Wave-front curvature as a cause of slow conduction and block in isolated cardiac muscle. Circ Res 1994;75:1014–28.

Cinelli AR, Salzberg BM. Multiple site optical recording of transmembrane voltage (MSORTV), single-unit recordings, and evoked field potentials from the olfactory bulb of skate (*Raja erinacea*). J Neurophysiol 1990;64:1767–90.

Cinelli AR, Salzberg BM. Dendritic origin of late events in optical recordings from salamander olfactory bulb. J Neurophysiol 1992;68:786–806.

Cohen LB, Lesher S. Optical monitoring of membrane potential: methods of multisite optical measurement. In: DeWeer P, Salzberg BM, editors. Optical Methods in Cell Physiology. New York: Wiley, 1986. p. 71–99.

Davenport WB, Root WL. An introduction to the theory of random signals and noise. New York: McGraw-Hill, 1958. p. 112–144.

Falk CX, Wu JY, Cohen LB, Tang AC. Nonuniform expression of habituation in the activity of distinct classes of neurons in the Aplysia abdominal ganglion. J Neurosci 1993;13:4072–81.

Frostig RD, Lieke EE, Ts'o DY, Grinvald A. Cortical functional architecture and local coupling between neuronal activity and the microcirculation revealed by in vivo high-resolution optical imaging of intrinsic signals. Proc Natl Acad Sci USA 1990;87:6082–6.

Gogan P, Schmiedel-Jakob I, Chitti Y, Tyc-Dumont S. Fluorescence imaging of local membrane electric fields during the excitation of single neurons in culture. Biophys J 1995;69:299–310.

Grinvald A, Anglister L, Freeman JA, Hildesheim R, Manker A. Real-time optical imaging of naturally evoked electrical activity in intact frog brain. Nature 1984;308:848–50.

Grinvald A, Cohen LB, Lesher S, Boyle MB. Simultaneous optical monitoring of activity of many neurons in invertebrate ganglia using a 124-element photodiode array. J Neurophysiol 1981;45:829–40.

Hirota A, Sato K, Momose-Sato Y, Sakai T, Kamino K. A new simultaneous 1020-site optical recording system for monitoring neural activity using voltage-sensitive dyes. J Neurosci Methods 1995;56:187–94.

Ichikawa M, Iijima T, Matsumoto G. Real-time optical recording of neural activities in the brain. In: Ono T, Squire LR, Raichle ME, Perrett DI, Fukuda M, editors. Brain mechanisms of perception and memory. New York: Oxford University Press, 1993. p. 638–648.

Iijima T, Matsumoto G, Kidokoro Y. Synaptic activation of rat adrenal medulla examined with a large photodiode array in combination with a voltage-sensitive dye. Neuroscience 1992;51:211–9.

Iijima T, Witter MP, Ichikawa M, Tominaga T, Kajiwara R, Matsumoto G. Entorhinal–hippocampal interactions revealed by real-time imaging. Science 1996;272:1176–9.

Kauer JS, Senseman DM, Cohen LB. Odor-elicited activity monitored simultaneously from 124 regions of the salamander olfactory bulb using a voltage-sensitive dye. Brain Res 1987;418:255–61.

Kleinfeld D, Delaney KR, Fee MS, Flores JA, Tank DW, Gelperin A. Dynamics of propagating waves in the olfactory network of a terrestrial mollusc: an electrical and optical study. J Neurophysiol 1994;72:1402–19.

Kogan A, Ross WN, Zecevic D, Lasser-Ross N. Optical recording from cerebellar Purkinje cells using intracellularly injected voltage-sensitive dyes. Brain Res 1995;700:235–9.

Lasser-Ross N, Miyakawa H, Lev-Ram V, Young SR, Ross WN. High time resolution fluorescence imaging with a CCD camera. J Neurosci Methods 1991;36:253–61.

London JA, Cohen LB, Wu JY. Optical recordings of the cortical response to whisker stimulation before and after the addition of an epileptogenic agent. J Neurosci 1989;9:2182–90.

Nakashima M, Yamada S, Shiono S, Maeda M, Satoh F. 448-detector optical recording system: development and application to Aplysia gill-withdrawal reflex. IEEE Trans Biomed Eng 1992;39:26–36.

Orbach HS, Cohen LB. Optical monitoring of activity from many areas of the in vitro and in vivo salamander olfactory bulb: a new method for studying functional organization in the vertebrate central nervous system. J Neurosci 1983;3:2251–62.

Orbach HS, Cohen LB, Grinvald A. Optical mapping of electrical activity in rat somatosensory and visual cortex. J Neurosci 1985;5:1886–95.

Potter SM, Mart A, Pine J. High-speed CCD movie camera with random pixel selection for neurobiology research. Proc SPIE 1997;2869:243–53.

Ratzlaff EH, Grinvald A. A tandem-lens epifluorescence macroscope: hundred-fold brightness advantage for wide-field imaging. J Neurosci Methods 1991;36:127–37.

Salzberg BM, Obaid AL, Senseman DM, Gainer H. Optical recording of action potentials from vertebrate nerve terminals using potentiometric probes provides evidence for sodium and calcium components. Nature 1983;306:36–40.

Ts'o DY, Frostig RD, Lieke EE, Grinvald A. Functional organization of primate visual cortex revealed by high resolution optical imaging. Science 1990;249:417–20.

Wong-Riley M. Changes in the visual system of monocularly sutured or enucleated cats demonstrable with cytochrome oxidase histochemistry. Brain Res 1979;171:11–28.

High-speed, high-resolution epifluorescence imaging system using CCD sensor and digital storage for neurobiological research

Ichiro Takashima[1], Riichi Kajiwara[1], Kiyo Murano[1], Toshio Iijima[1],
Yasuhiro Morinaka[2] and Hiroyoshi Komobuchi[2]

[1]Supermolecular Science Division, Electrotechnical Laboratory,
1-1-4 Umezono, Tsukuba, Ibaraki 305-8568 Japan
[2]Advanced Technology Research Laboratory, Matsushita Electric Industrial Co., Ltd.
3-4 Hikaridai, Seika, Souraku, Kyoto 619-0237 Japan

ABSTRACT

We have designed and built a high-speed CCD imaging system for monitoring neural activity in an exposed animal cortex stained with a voltage-sensitive dye. Two types of custom-made CCD sensors were developed for this system. The type I chip has a resolution of 2664 (H) × 1200 (V) pixels and a wide imaging area of 28.1 × 13.8 mm, while the type II chip has 1776 × 1626 pixels and an active imaging area of 20.4 × 18.7 mm. The CCD arrays were constructed with multiple output amplifiers in order to accelerate the readout rate. The two chips were divided into either 24 (I) or 16 (II) distinct areas that were driven in parallel. The parallel CCD outputs were digitized by 12-bit A/D converters and then stored in the frame memory. The frame memory was constructed with synchronous DRAM modules, which provided a capacity of 128 MB per channel. On-chip and on-memory binning methods were incorporated into the system, e.g., this enabled us to capture 444 × 200 pixel-images for periods of 36 seconds at a rate of 500 frames/second. This system was successfully used to visualize neural activity in the cortices of rats, guinea pigs, and monkeys.

Keywords: voltage-sensitive dye, fluorescence, optical recording, neural activity, somatosensory cortex, motor cortex, digital image storage

1. INTRODUCTION

The unraveling of biological enigmas in the brain has become one of the most challenging frontiers of science. In order to understand the brain, long-term joint research has been carried out in several diverse fields, including electrophysiology, anatomy, biochemistry, genetics, psychophysics, neurology, and computational theory. Nevertheless, very little is yet known about how various parts of the brain interact and how this interaction allows us to read, walk, and respond to stimuli. This can be partly attributed to the gap between the immense complexity of the brain and the limited capabilities of currently available research tools. A major obstacle in brain research is the difficulty in monitoring dynamic patterns of neural activity at millisecond time intervals. Therefore, our understanding of brain functions may be enhanced through more detailed monitoring of brain activity. Any useful method for this monitoring should have (1) sufficient time resolution to trace the electrical activity of neurons (< several ms), (2) sufficient spatial resolution to resolve cortical functional units (< 100 μm), and (3) the ability to simultaneously monitor neural activity at many sites. The optical imaging technique described in this paper is one potential method that satisfies these demands.

Over the last two decades, it has become possible to detect and measure rapid transient changes in neuron membrane potential by using voltage-sensitive dyes as optical probes. Changes in the absorption or fluorescence of these dyes when bound to membranes are proportional to the voltage changes across that membrane. The optical signals of certain potentiometric dyes follow changes in the membrane potential with a delay of less than 0.01 ms (for reviews see Cohen and Salzberg [1] and Grinvald et al.[2]). An array of photodetectors can be used to project an image of the dye-stained brain. Monitoring output of these photodetectors results in a simultaneous measure of the average membrane potential of the neuron ensemble. This shows how groups of neurons interact to control behavior or to form specific synaptic connections.

Early efforts at multiple-site optical recordings used 12 × 12- or 16 × 16-element photodiode matrix arrays [3, 4], because only photodiodes have proven to be sufficiently sensitive and fast for imaging voltage-sensitive dyes. While these photodiode sensor arrays had high temporal resolution, their spatial resolution was intrinsically limited. Since then, higher spatial resolution has been achieved using a MOS-based solid-state camera [5], or high-speed CCD cameras [6, 7, 8]. These cameras have been successfully utilized to monitor dynamic patterns of electrical activity from a variety of preparations [9, 10]. However, the active imaging areas of these cameras were quite small, which conflicts with our requirement that the cameras simultaneously cover large areas of the cortex. The small coverage area of these cameras was a consequence of the desire to have a high-speed readout of pixels. Moreover, it is difficult to design a tandem-lens epifluorescence macroscope used for imaging [11] with a magnification less than 1 ×. Typically, an imaging area larger than 10 mm square is required for large animals, such as monkeys.

In order to achieve our goal of wide area coverage, we designed an optical imaging system using custom-made CCD chips that have an imaging area over 10 mm per side. High-speed imaging at 500 frames/second with a spatial resolution of 444 × 200 pixels was attained by using parallel processing of multiple CCD outputs and by incorporating an on-chip binning method. This paper describes the essential design details of our imaging system and presents some demonstrative data for neurobiological research.

2. CCD ARCHITECTURE

We developed two types of CCD devices based on interline transfer architecture. As shown in Fig. 1 (A), the type I chip is divided into 24 distinct areas (channels) driven in parallel; each area is composed of 111 (H) × 1200 (V) pixels and an output amplifier. A slant down VCCD design (in the form of 111 × 24) makes it possible to place a readout amplifier between two adjacent HCCDs, which allows a completely parallel arrayed CCD structure. The chip employs 24-phase and 2-phase clocking for the vertical and horizontal charge shift operations, respectively. The type I chip is oblong and the total pixel area is 2664 (H) × 1200 (V). To avoid image discontinuity, we used both end channels as optical black channels rather than place optical black pixels at channel borders, as typically done. Channels 1 and 24 are optically overshadowed and the dark level is used as a reference, which may be required for dark level compensation between channels. Therefore, channels 2 to 23 constitute a wide 28.1 × 13.8 mm imaging area. On the other hand, the type II chip is divided into 16 channels each of which has 111 (H) × 1626 (V) pixels, as shown in Fig. 1 (B). The type II chip architecture is similar to the type I except that it has a reduced number of channels and has vertically elongated picture elements. Since all sixteen type II channels can be used for imaging, an aggregate of 1776 (H) × 1626 (V) pixels creates an active imaging area of 20.4 × 18.7 mm. A photograph of the two CCD types is shown in Fig. 2.

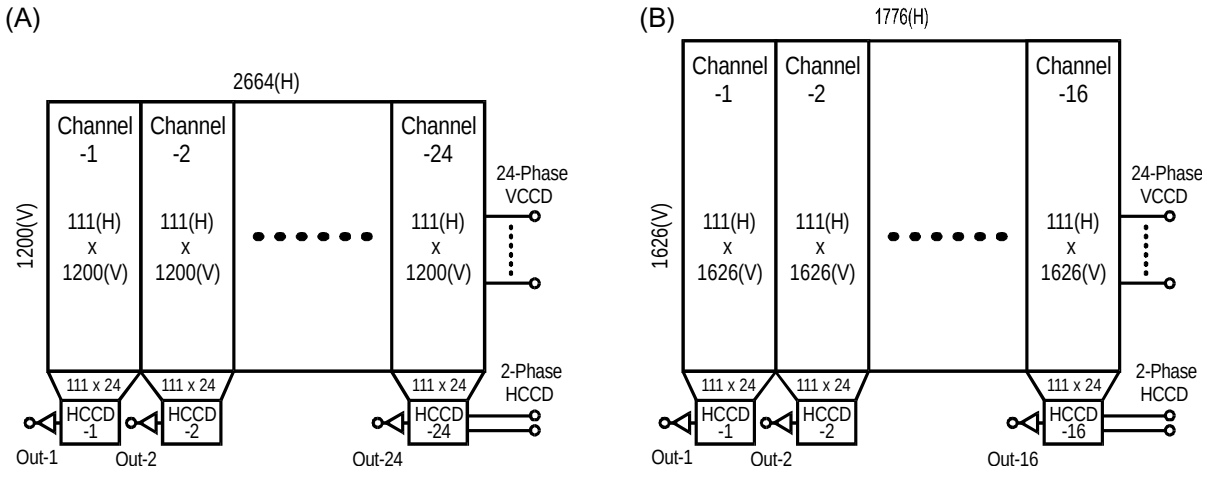

Fig. 1. Design schematic of the CCD devices. Type I (A) and Type II (B) chips.

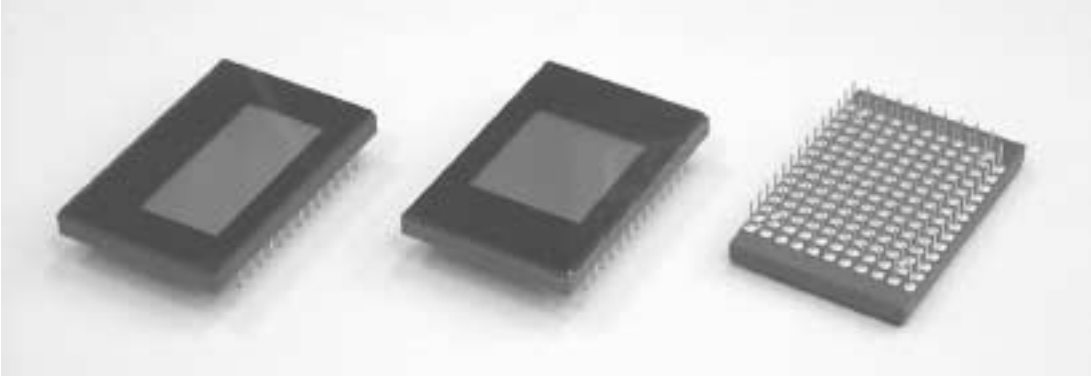

Fig. 2. Photograph of the CCD devices. Type I (left) and Type II (center) chips in 53-pin Ceramic PGA packages and their bottom view (right). The package dimensions are 42 × 28 × 4 mm.

The 24-phase VCCD driving pulses provided a variety of readout operations including progressive or interlace scanning and on-chip binning. The chip output voltage showed a wide dynamic range of 2Vp-p saturation. As described in the following section, it is normally programmed to combine six vertically adjacent pixels into one super-pixel, i.e., a 1 (H) × 6 (V)-binning, for the optical imaging system. As a result of this on-chip binning, the type I and II chips produced images at a rate exceeding 500 and 400 frames/second, respectively.

Please refer to our accompanying paper entitled "8-ch parallel readout high-speed wide dynamic range CCD" for more detailed CCD design considerations [12].

3. SYSTEM DESIGN

Our optical imaging system was built around the CCD chips described in the previous section. The system is composed of a camera unit, an optical apparatus, and a PC/AT computer. The camera unit is composed of two printed circuits boards, termed the head board and processor board. The CCD chip is mounted on the head board. The multiple CCD outputs are digitized in the head board and successively fed to the processor board where a group of frame memories is symmetrically formed. The image data stored in the frame memories is then transferred to the computer via RS-422 line drivers. The tandem-type macroscope, which the camera unit can be attached to, was also designed for our system.

3.1. Head Board

The head board was designed to be compatible with both type I and type II CCD chips. The head board block diagram is shown in Fig. 3. We used two types of programmable devices, a field program gate array (FPGA) and a programmable timing controller (PTC), in order to generate the clocks required to drive the CCD. The multiple CCD outputs are processed in parallel through correlated double sampling (CDS), the dark level clamping circuits (Clamp), amplification, and the A/D converters (ADC). Each channel has its own discrete daughter board set, consisting of a CDS, clamp, amplifier, and ADC circuits, fabricated and attached to the head board via a connector. Therefore, twenty-four daughter boards were used for the type I CCD chip, while sixteen boards were used for the type II chip. The FPGA (EPF10K30E-TC144, Altera, San Jose, CA) generated 2-phase driving pulses for the HCCDs (H1/H2/R), sampling pulses for the CDS circuits (DS1/DS2), clamp pulses, and conversion pulses for the ADCs. The HCCDs were driven at 24 MHz while a clock of its fourfold frequency (96 MHz) was connected to the FPGA. The PTC (TMS57106PCE, Texas Instruments, Dallas, TX) generated 24-phase driving pulses for the VCCDs together with the V-driver chips (MN3112SA, Panasonic, Osaka, Japan). The PTC also generated vertical and horizontal synchronization pulses, VD and HD. Although the VCCDs could be driven by the 24-phase pulses, we drove them at 0.25 MHz by using reduced 8-phase pulses and combining six vertically adjacent pixels. As a result of this on-chip binning, each type I chip channel produced 111 (H) × 200 (V) pixel-images at a maximum rate of 544 frames/second while the type II chip produced 111 (H) × 271 (V) pixel-images at a maximum rate of 404 frames/second.

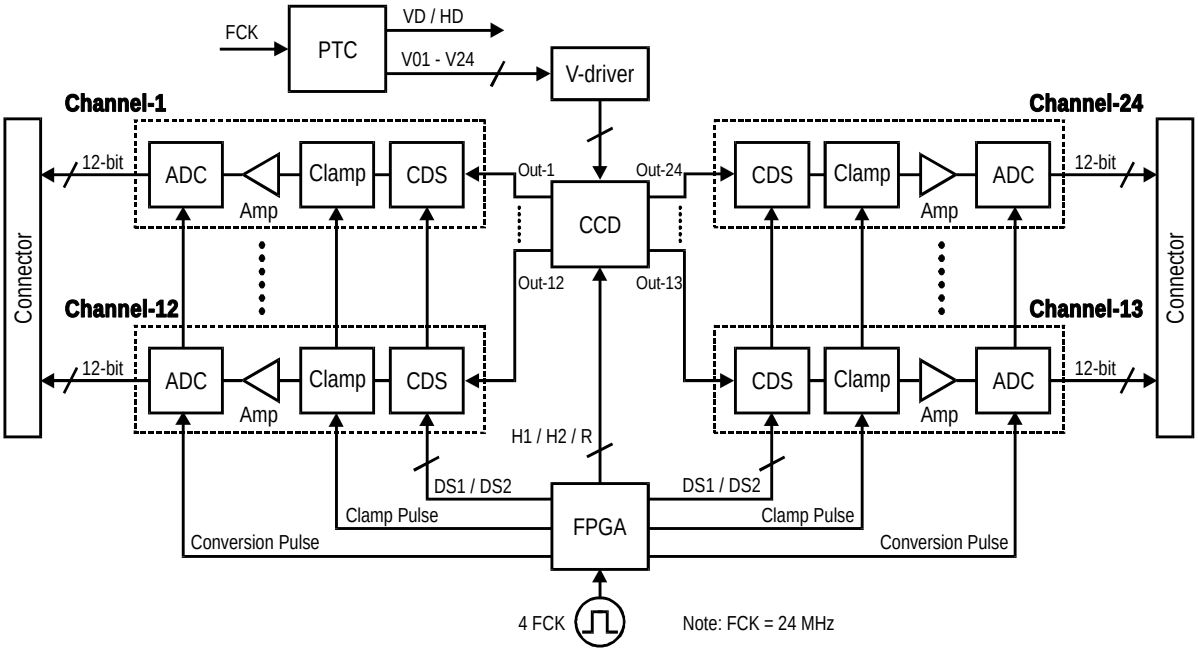

Fig. 3. Head Board Block diagram

The correlated double sampling function was implemented using the CDS chip (AN2108NFHQ, Panasonic, Osaka, Japan), which could sample video signals at a rate exceeding 30 MHz. The auto gain control (AGC) and gamma correction functions were also incorporated into the CDS chip; however, we chose to disable these redundant functions for our optical imaging system. The clamp circuit clamped the signal D.C. level to certain fixed voltages when the clamp pulse was received during the horizontal blanking periods. Each channel had adjustable and independent clamp voltages and amplifier gains that allowed for compensation for any differences in adjacent channel output characteristics. The output signals were finally converted to digital signals by a high-speed ADC (AD9224ARS, Analog Devices, Norwood, MA). This ADC was a 12-bit track-and hold A/D converter and had the ability to provide digital output at 40 MSPS. The digitized data was fed to the processor board via connectors. As shown in Fig. 3, channels 1-12 and channels 24-13 were arranged on the head board symmetrically with respect to the CCD chip. The type II CCD chip used sixteen outputs from channels 5-20 and the residual channels 1-4 and 24-21 were idled in Fig. 3. Fig. 5 shows a photograph of the head board.

3.2. Processor Board

A block diagram of the processor board is shown in Fig. 4. The processor board can be fixed to the head board via connectors; the connectors at each end in Fig. 4 correspond to those in Fig. 3. The processor board used timming clocks, such as 2FCK, VD and HD, generated on the head board; hence, the synchronous operation of the two separated printed circuit boards was ensured. The processor board formed a group of frame memories. The frame memory for each channel was composed of an FPGA device (EPF10K30ATC144, Altera), shown as the memory FPGA in Fig. 3, and synchronous DRAM (SDRAM) chips (KM44S16020A, Samsung, Seoul, Korea). Sixteen SDRAM chips were utilized per channel, for a total capacity of 128 MB (64-Mword × 16-bit), and they were divided into four blocks. The memory FPGA device received 12-bit digitized data sequentially and wrote it to the four SDRAM blocks in turn. Since the FPGA managed each SDRAM block independently, it enabled burst writing of data to a specific block and the simultaneous refreshing of the remaining blocks. Each channel's frame memory was fabricated as a discrete memory board and could be fitted into a 168-pin DIMM socket that was installed on the processor board. The future requirement for a larger capacity frame memory may be realized by redesigning and replacing the memory board. Channel groups 1-12 and 13-24 were processed in parallel on the processor board. Two FPGA devices (EPF10K50VRC240, Altera), indicated by A-FPGA and B-FPGA in Fig. 3, controlled the frame memory for channels 1-12 and 13-24, respectively. The hardware logic circuits implemented in these two FPGA devices

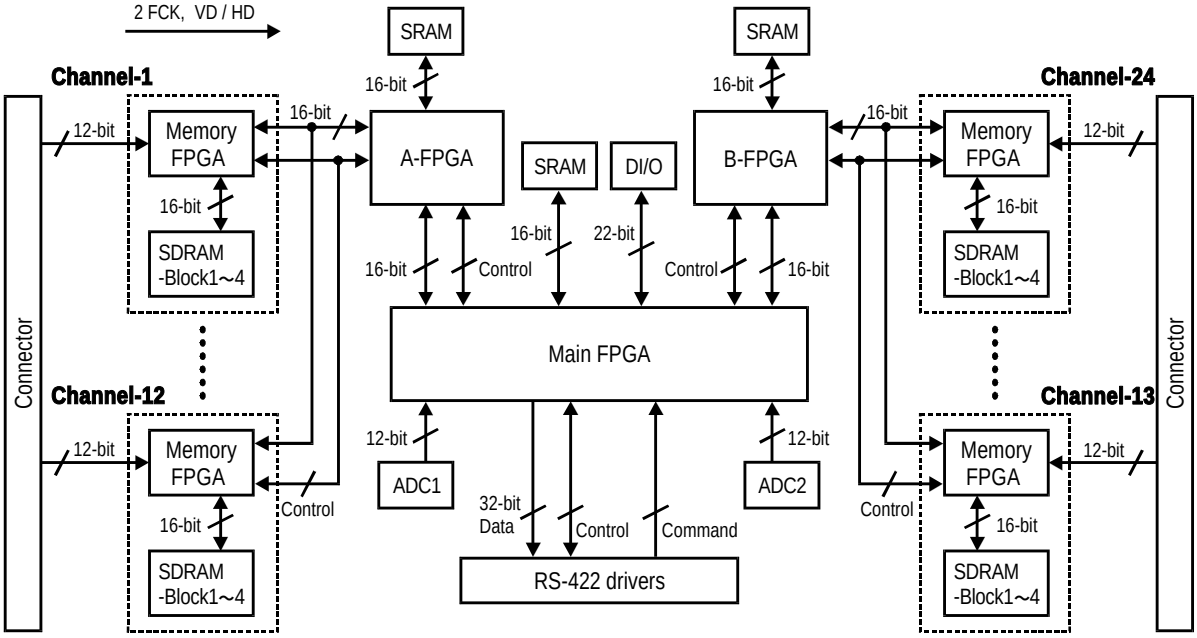

Fig. 4. Processor Board Block diagram

were identical. The basic function of the A/B-FPGA devices was to receive 16-bit data from the memory board by polling each channel and then transferring the data to another FPGA, called the main FPGA in Fig. 3. The A/B-FPGA supplied 256 kB of local SRAM working memory. This SRAM was used as temporary memory for digital data processing. Specifically, the FPGAs moved some image data from the frame memory to the SRAM, performed some image processing, and wrote the data back to the frame memory. The data traffic occupied a 16-bit width between the A/B-FPGA and other devices, i.e., the memory FPGA, the SRAM, and the main FPGA. The main FPGA (EPF10K50VBC356, Altera) received 16-bit data from both the A-FPGA and B-FPGA simultaneously. Both sets of 16-bit data were subsequently concatenated into one 32-bit data stream and transferred to the computer. Due to both the symmetrical design of the processor board and the parallel processing of the two channel groups, image data that corresponded to channel-i and channel-(25-i), where i = 1-12, could be concatenated in the main FPGA.

The main FPGA device communicated with the computer. At times, it was necessary to leave the camera unit in the darkroom with the animals during optical imaging experiments, while the computer was in an adjoining room. Therefore, RS-422 differential line drivers (DS90C031/032, National Semiconductor, Santa Clara, CA) and twisted-pair cables (20 m long) were used for both command and image data transmission. We used a variety of camera control commands for the experiments, e.g., parameter, acquisition, and download commands. The parameter command included imaging parameters, such as the number of frames to be acquired, the trigger mode, the number of trials to be averaged, the interval between trials, and the write-start address of the frame memory. The acquisition command initiated image acquisition, storing a series of images in the SDRAM. The download command transferred image data in the frame memory to the computer in the form of 32-bit concatenated data.

The main FPGA device has a digital input/output (DI/O) function. The digital outputs were used to control the electric stimulator and the mechanical shutter. In order to evoke and monitor neural activity, weak electric stimulation was applied to the brain during the continuous image capture period. It was necessary to place a shutter between the brain and the light source, as some voltage-sensitive dyes are toxic to neurons if too much light is absorbed. The shutter was commanded to open just before image capture and to close immediately after image acquisition. The digital input was used to sense an external trigger pulse, such as electrocardiograph output. This enabled image acquisition to be synchronized with the electrocardiogram of the animal. Two multi-channel ADCs (AD7864, Analog Devices), indicated as ADC1 and ADC2 in

Fig. 4, were equipped for digital sampling of the analog signals recorded during optical imaging. These signals could include field potentials, electrocardiograms, and so on. The ADC was a simultaneously sampling, four-channel, 12-bit A/D converter with a maximum throughput of 500 kSPS. The main FPGA sent conversion pulses to the ADCs during the horizontal blanking periods and the ADC digital output signals were incorporated into the imaging data. The main FPGA uses SRAM as its local working memory.

In addition to the CCD on-chip binning, our system also incorporated an on-memory binning method. On-memory binning was implemented because of the (1) balanced vertical/horizontal spatial resolution and (2) wide dynamic range of digital data for each pixel. Since the on-chip binning format is 1 (H) × 6 (V), we selected the on-memory binning formats of 6 (H) × 1 (V) or 8 (H) × 1 (V). The 6 × 1 on-memory binning format, in combination with the 1 × 6 on-chip binning format, produced a type I CCD imaging system with a resolution of 444 (H) × 200 (V) pixels and a type II CCD system with a resolution of 296 × 271 pixels. The on-memory binning process was performed for the ADC 12-bit output data. Therefore, the 8 (H) × 1 (V) on-memory binning format increased the bit resolution per pixel by 3 bits to 15 bits. The wider pixel dynamic range provided a finer sensitivity for detecting neural activity during optical imaging. This was because fractional changes in dye epifluorescence are associated with changes in the transmembrane potential of the neuron ensemble. Both the memory FPGA and A/B-FPGA devices in Fig. 4 performed on-memory binning.

We used two download modes to transfer image data from the camera unit to the computer. In the basic mode, raw data stored in the frame memory were transferred without any processing while the frame difference image was transferred during the subtraction mode. Optical imaging of neural activity was achieved by subtracting the R-image from the A-image, where the R-image and A-image were obtained during periods of rest and activity in the brain, respectively. In the subtraction mode, each image was successively subtracted from the reference background image and transmitted to the computer. The image subtraction procedure was performed by the A/B-FPGA devices in Fig. 4. An insufficient SNR for one-shot optical imaging would necessitate considering a trial averaging method. Trial averaging was done by either the memory FPGA in real time or by the A/B-FPGA during download. A photograph of the U-shaped processor board is shown in Fig. 5.

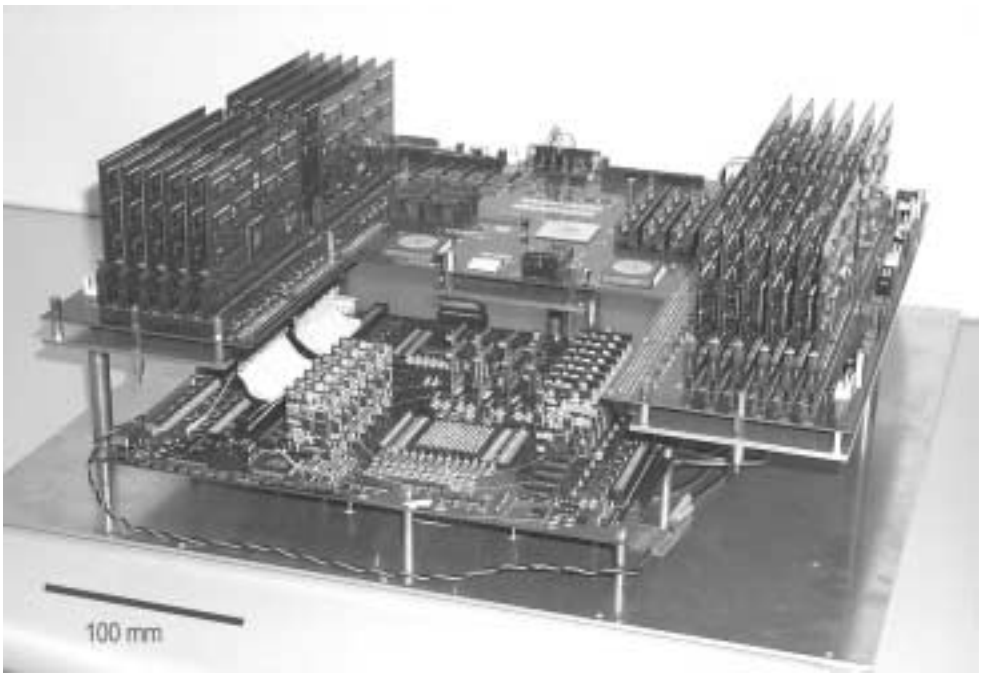

Fig. 5. Photograph of the camera unit. The top and side walls of the camera box are removed to show its interior. The processor board (Upper) is placed on top of the head board (Lower).

3.3. Computer and Software

A PC/AT computer was used for camera unit control, camera image data reception, and real time visualization of neural activity. The PC/AT parallel (printer) port was used to send control commands to the camera. A high-speed, 32-bit parallel input/output board (GPIO-100M, Graphin, Tokyo, Japan) was used to receive the 32-bit image data from the camera. This PCI board enabled data capture to be synchronized with the externally supplied transmission clock (24 MHz).

A software package was developed in a window-based MDI/GUI environment (Microsoft Visual C++ 6.0), as shown in Fig. 6. This package allowed convenient command and control of the camera unit and offered software tools for collecting, processing, displaying, storing, analyzing, and printing the optical imaging data.

3.4. Optical Apparatus

The optical apparatus, designed and constructed in our laboratory, is similar to the tandem type epifluorescent macroscope of Ratzlaff and Grinvald [11]. An outline of the apparatus is shown in Fig. 7 (A). The lamp house and tandem lenses are attached to the mechanical XYZ-TF stage driven by pulse-motors. The stage controller is shown in Fig. 7 (C). Since the mechanical stage itself weighs about 110 kg, it is secured to the frame base. A monkey sitting on a monkey-chair can easily be put into the frames and placed under the objective lens. A tungsten-halogen lamp is set in the lamp house and voltage-stabilized DC power is supplied. A CD-ROM case placed above the lens in Fig. 7 (A) helps to show the optical apparatus scale. The bottom of the camera unit (Fig. 5) can be attached to the upper part of the cylindrical container of the imaging

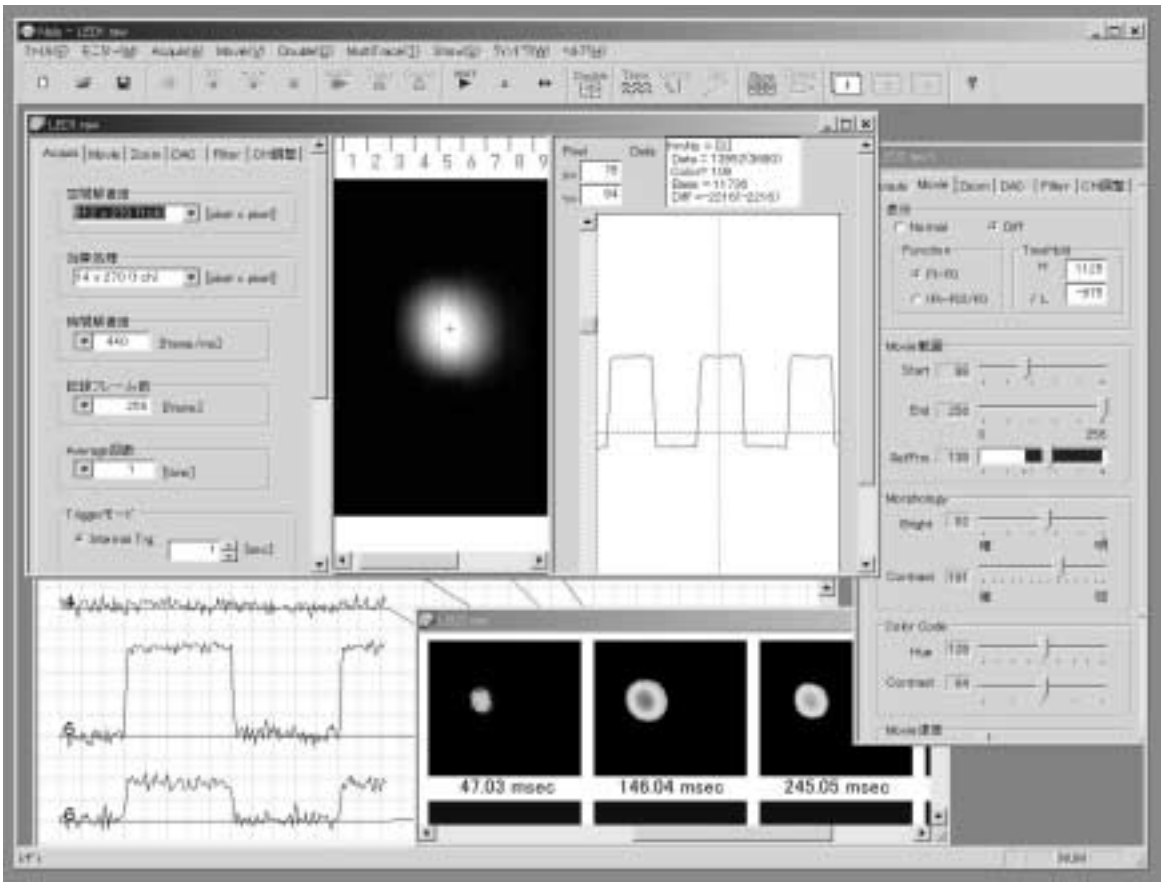

Fig. 6. A software package developed for optical imaging. See Sections 3.3 and 4.2.

lens, where the CD-ROM case is shown in Fig. 7 (A). Two types of custom-made lenses are shown in Fig. 7 (B) and were designed to have a nearly uniform illumination over the wide CCD active area. The first lens was f = 50 mm, N.A. = 0.5 (F/1), focal depth = 12 μm, MTF > 0.2 (50 lp/mm), and provided 90 % illumination at 5.5 mm off-axis. The second lens was f = 101 mm, N.A. = 0.3 (F/1.7), focal depth = 20 μm, MTF > 0.2 (25 lp/mm), and provided 95 % illumination at 13 mm off-axis. The first and second lenses weighed about 4.0 and 2.5 kg, respectively. In the tandem lens system, the magnification was simply the ratio of the focal lengths of the primary (objective) and secondary (imaging) lenses. Using f = 101 mm lenses for both the objective and imaging lens resulted in 1 × magnification. A combination of an f = 50 mm objective lens and an f = 101 mm imaging lens provided 2 × magnification.

We normally used the voltage-sensitive dye RH-795 (Molecular Probes, Eugene, OR) for optical imaging. It has excitation and emission maxima at 530 and 712 nm, respectively. Therefore, illumination from the halogen lamp was filtered at 535 nm (±20 nm bandpass) and reflected onto the preparations by a dichroic mirror (half-reflectance wavelength of 580 nm). The fluorescence from the preparations was collected by the objective lens and projected through the dichroic mirror, a long-wavelength pass filter (50% transmittance at 600 nm), the imaging lens, and finally onto the CCD sensor. The interference filters used in the apparatus are shown in Fig. 7 (B).

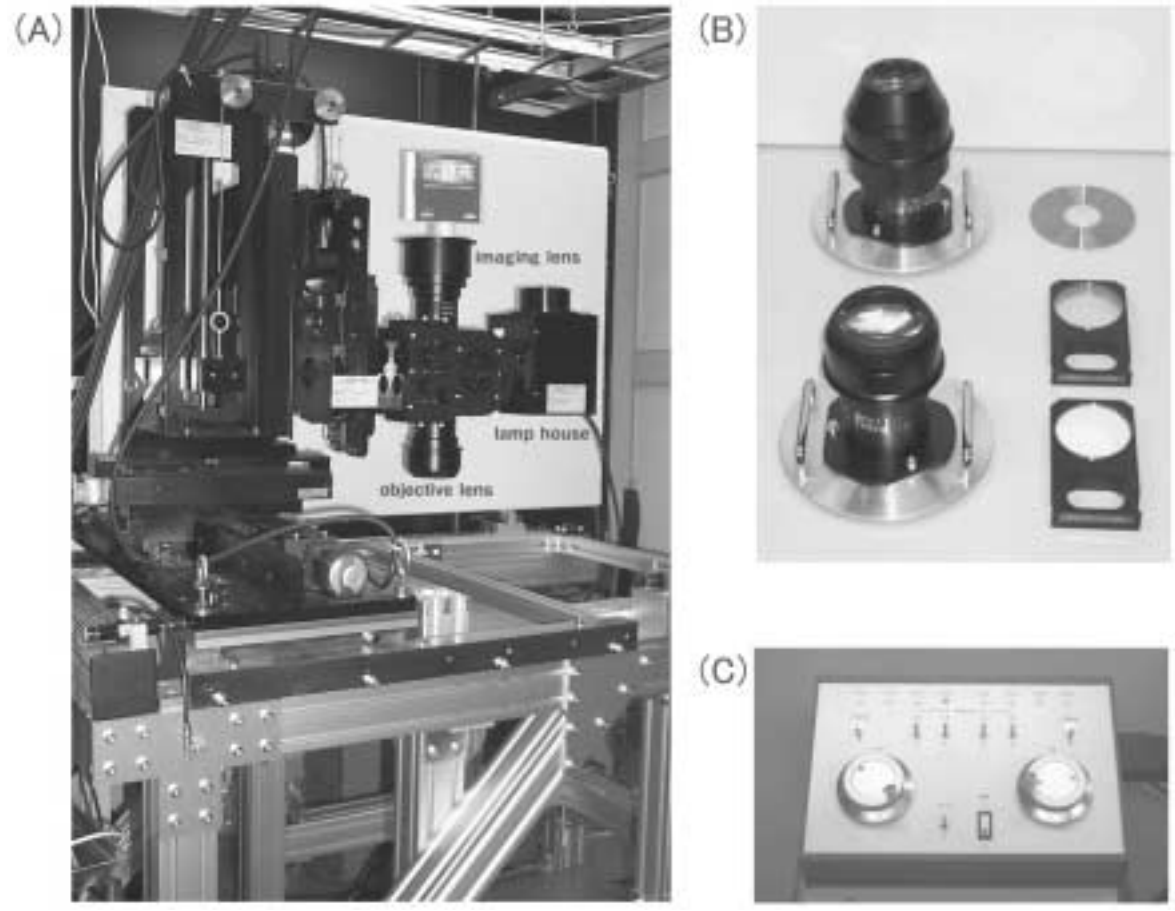

Fig. 7. Photograph of the optical apparatus.

(A) A cover shot of the apparatus. (B) Custom made f = 50 mm (upper left) and f = 101 mm (lower left) lenses and interference filters (middle and lower right). A CD-ROM (upper right) is shown for scale. (C) The controller for the mechanical XYZ-TF stage.

4. SYSTEM PERFORMANCE

4.1. Spatiotemporal Resolution

We verified the normal operation of the CCD horizontal shift registers and output amplifiers at up to 25 MHz [12]. It was easy to change the on-chip binning format geometry by downloading the appropriate hardware logic to the programmable devices. Therefore, we could have pursued the maximum performance of our imaging system; however, we chose to fix and implement the HCCD 24 MHz clock and the 1 (H) × 6 (V) on-chip binning format for our study. We chose this method because a clock frequency of 24 MHz allowed for simplified handling, A/D hardware circuit design, SDRAM access, and PCI data transmission to the computer. Therefore, the 24 MHz clock was used as a global clock for both analog and digital circuits in the camera unit. Moreover, each channel has 111 horizontal pixels, a number whose only divisor is 3. This is why we selected a binning of 6 (V), as it is a multiple of 3.

Table I summarizes the system performance of our imaging system.

4.2. Detection of Brief and/or Slight Changes in Light Intensity

As the voltage-sensitive dye transforms neural activity into fractional change in fluorescence, any useful optical imaging apparatus must have a system that can detect brief or slight changes in light intensity with a sufficient SNR and have no lag. As mentioned in the previous section, Fig. 6 shows the results of a step change in a light emitting diode's (LED) light intensity as monitored by our imaging system. The lower left window in Fig. 6 shows traces of light intensity change, as detected by a single pixel, when the LED electric current was changed about 0.5 % over a period of 200 ms. The step change in the light intensity is clearly traced. This result suggests that a 0.5 % fluorescence change in the voltage-sensitive dye should be successfully detected by our system because (1) the LED used has similar emission wavelengths to the dye fluorescence, and (2) in this experiment there was a linear relationship between the supplied electric current driving the LED and light intensity.

The system should have a 1 ms or shorter time resolution in order to trace the electrical activity of single neurons. However, the ~2 ms resolution of our system should be sufficient for our study, since we examined the cortical response or population activity of an ensemble of neurons. The maximum fractional change in fluorescence of the voltage-sensitive dye RH-795 *in vivo* is ~0.1 %, which is equivalent to 5-bit resolution when each pixel has a 15-bit width after 8 × 1 format on-memory binning. Since a 5-bit dynamic range seems insufficient for detecting small changes in dye fluorescence, we implemented a contrast enhancement technique in the analog domain by placing an offset bias and amplifier circuits before the ADCs [13].

Table 1. Performance characteristics of the imaging system.

	On-chip binning format	CCD readout pixels after on-chip binning	Frame rate (frames/sec)	On-memory binning format	Spatial resolution after on-memory binning	Dynamic range of one pixel (bit)	Number of storable frames
Type I CCD chip	1 x 6	2664 x 200 (111 x 200 / CH)	544	6 x 1	444 x 200 (Active: 407 x 200)	~ 14.6	17660
				8 x 1	333 x 200 (Active: 305 x 200)	15	22369
Type II CCD chip	1 x 6	1776 x 271 (111 x 271 / CH)	404	6 x 1	296 x 271	~ 14.6	13033
				8 x 1	222 x 271	15	16508

5. NEUROBIOLOGICAL APPLICATION

5.1. Neural Activity in the Rodent Somatosensory Cortex

Male guinea pigs (~180 g) were anesthetized with an intraperitoneal injection of Nembutal (20 mg/kg). The head of the animal was fixed in a stereotaxic apparatus and a craniotomy was performed over both the right and left somatosensory cortices. A well of dental acrylic was built around the exposed cortices, the dura matter was removed, and the cortical surface was stained with a voltage-sensitive dye RH-795 (0.6 mg/ml) for ~1 hour. The dye was then fully washed out and the well was filled with artificial cerebrospinal fluid. The animal was placed under the objective lens and an electrical stimulation (200 μs duration, 500 μA intensity) was applied to the right whisker pads of the animal's snout. In the optical imaging experiments, the dye epifluorescence was detected by the system, which was synchronized to the stimulation, and the fractional change was calculated for functional imaging. Fig. 8 shows the imaging results of evoked neural activity in the somatosensory cortices. The type II CCD chip was used in these experiments.

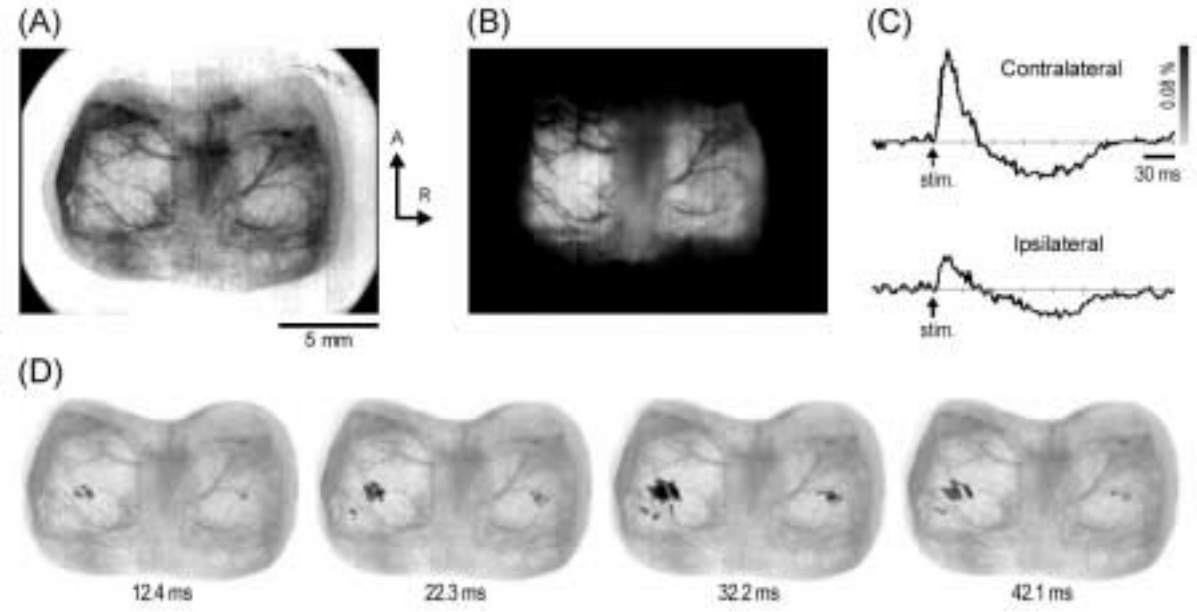

Fig. 8. *In vivo* optical imaging of evoked neural activity in the somatosensory cortices of guinea pigs.

(A) The surface image of the brain under ordinary illumination (A: anterior, R: right). The skull openings in both cerebral hemispheres are about 5 mm square and symmetric with respect to the sagittal suture. A well of dental acrylic was built around the exposed brain. The image is composed using fourteen of the sixteen type II CCD channels and is trimmed at the upper and lower edges. (B) The fluorescent image of the cortical surface. The cortices are highlighted because the voltage-sensitive dye bound only to nervous tissue. The one hour staining procedure allowed the dye to penetrate ~1.0 mm into the cortex. (C) Optical signals detected by a single pixel in each hemisphere. Stimuli were given at 5-s intervals and sixteen trials were averaged. A decrease in fluorescence is plotted upward; therefore, an upward change in the trace reflects the membrane depolarization of cortical neuron ensembles, while a downward change represents the hyperpolarization of neurons. The depolarizing (excitatory) response peaked 20 ms after the stimulus onset and the hyperpolarizing (inhibitory) response followed. Neural activity in response to electrical stimulation at the right whisker pads was monitored in both hemispheres. The contralateral response (in the left hemisphere) was three times larger than the ipsilateral response (in the right hemisphere). (D) Spatio-temporal evolution of neural activity. The fractional change in fluorescence detected by each pixel was encoded in gray scale (the gray scale bar in C) and mapped onto the surface image of the brain. The post-stimulus times are indicated below each image.

5.2. Functional Mapping of the Monkey Somatosensory Cortex

We recorded neural responses to mechanical stimulation of a digit in the primary somatosensory cortex of monkeys (*Macaca fuscata*). The optical imaging procedure was much the same as described in the previous subsection. Under general anesthesia, we made a skull opening (~18 mm in diameter) over the right somatosensory cortex and attached a cylinder to the skull as shown in Fig. 9 (A). The dura matter was removed to expose the cortical surface and the cortex was stained with a voltage-sensitive dye RH-795 (0.5 mg/ml) for ~2 hours. The monkey was placed under the imaging system and each digit of his left hand was mechanically stimulated. Fig. 9 (B) shows the optical imaging of neural activity when digit two (D2) was stimulated. The somatotopically organized responses of D1, D3, and D5 are illustrated in Fig. 9 (C). The type II CCD chip was utilized in these experiments.

Recently, we succeeded in recording neural activity in the sensorimotor cortices of monkeys while they were performing a visually guided reaching task. Optical imaging revealed activated spots in the primary motor cortex as well as in the primary somatosensory cortex. For further details, see our recent publications [14, 15].

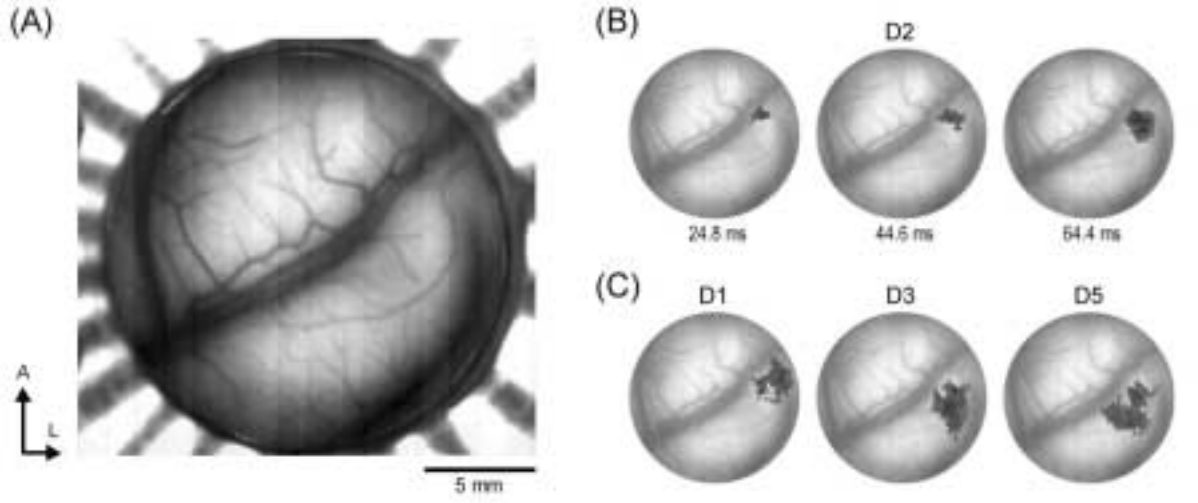

Fig. 9. *In vivo* optical imaging of neural activity in the somatosensory cortex of monkeys.

(A) The surface image of the recorded cortical area (A: anterior, L: lateral). The central sulcus separating the primary somatosensory cortex from the primary motor cortex is located in the middle of the view. The image is composed of sixteen type II CCD channels and covers an area of 20.4 × 18.7 mm. The concentric halation in the periphery of the image is from the metallic cylinder attached to the skull. (B) Spatio-temporal evolution of neural activity in response to D2 stimulation. Neural activity was encoded in gray scale and superimposed on the surface image. The post-stimulus times are indicated below each image. The response was initiated close to the central sulcus (Brodmann's area 3b) and spread in the postcentral gyrus (Brodmann's area 1). (C) Functional mapping of D1, D3, and D5 regions in the somatosensory cortex. Stimulation of each digit evoked somatotopically organized responses; the response to D1 stimulation was more lateral, while that to D5 stimulation was more medial. However, the responses to each digit-stimulation were highly overlapping.

CONCLUSIONS

A high-speed, high-resolution CCD imaging system was developed for optical imaging and examples of its application for neurobiological research are described in this report. In order to monitor neural activity that covers wide areas of the cortex, we enhanced our imaging system with the following improvements. (1) Extremely large format CCD chips with multiple outputs were designed. (2) High-speed (~2 ms) digital imaging was attained. (3) A large capacity frame memory was incorporated. (4) Hardware logic for digital image processing and data transmission to the PC was implemented. (5) Specially designed optical apparatus was set up. (6) Software tools for neurobiological experiments were prepared. Our imaging system has successfully visualized neural activities in animal brains and enabled us to analyze cooperative actions of different cortical areas. We have great expectations that our imaging system will become a powerful and very useful imaging tool for observing and revealing higher brain functions in future studies.

ACKNOWLEDGMENTS

This work was supported by the Agency of Industrial Science and Technology (AIST) of Japan and by the Japan Science and Technology Corporation (JST).

REFERENCES

1. L. B. Cohen and B. M. Salzberg, “Optical measurement of membrane potential,” Rev. Physiol. Biochem. Pharmacol. 83, pp.35-88, 1978
2. A. Grinvald, R. D. Frostig, E. Lieke and R. Hildesheim, “Optical imaging of neural activity,” Physiol. Rev. 68, pp.1285-1366, 1988
3. B. M. Salzberg, A. L. Obaid, D. M. Senseman and H. Gainer, “Opticalrecording of action potentials from vertebrate nerve terminals using potentiometric probes provides evidence for sodium and calcium components,” Nature 306, pp.36-40, 1983
4. T. Iijima, G. Matsumoto and Y. Kidokoro, “Synaptic activation of rat adrenal medulla examined with a large photodiode array in combination with a voltage-sensitive dye,” Neuroscience 51, pp.211-219, 1992
5. M. Ichikawa, T. Iijima and G. Matsumoto, “Real-time optical recording of neuronal activities in the brain,” In: *Brain Mechanisms of Perception and Memory*, T. Ono, L. R. Squire, M. E. Raichle, D. I. Perrett, M. Fukuda, editors, pp. 638-648, Oxford University Press, New York, 1993
6. N. Lasser-Ross, H. Miyakawa, V. Lev-Ram, S. R. Young and W. N. Ross, “High time resolution fluorescence imaging with a CCD camera,” J. Neurosci. Methods 36, pp.253-261, 1991
7. S. M. Potter, A. N. Mart and J. Pine, “High-speed CCD movie camera with random pixel selection, for neurobiology research,” Proc. SPIE 2869, pp. 243-253, 1997
8. I. Takashima, M. Ichikawa and T. Iijima, “High-speed CCD imaging system for monitoring neural activity *in vivo* and *in vitro*, using a voltage-sensitive dye,” J. Neurosci. Methods 91, pp.147-159, 1999
9. T. Iijima, M. P. Witter, M. Ichikawa, T. Tominaga, R. Kajiwara and G. Matsumoto, “Entorhinal-hippocampal interactions revealed by real-time imaging,” Science 272, pp.1176-1179, 1996
10. M. de Curtis, I. Takashima and T. Iijima, “Optical recording of cortical activity after in vitro perfusion of cerebral arteries with a voltage-sensitive dye,” Brain Res. 837, pp.314-319, 1999
11. E. H. Ratzlaff and A. Grinvald, “A tandem-lens epifluorescence macroscope: hundred-fold brightness advantage for wide-field imaging,” J. Neurosci. Methods 36, pp.127-137, 1991
12. Y. Morinaka, H. Komobuchi, S. Suzuki and T. Yamaguchi, “8-ch parallel readout high-speed wide dynamic range CCD,” Proc. SPIE 4183-2, 2000
13. S. Inoue and K. R. Spring, *Video Microscopy : The Fundamentals*, Plenum Press, New York, 1997
14. T. Iijima, I. Takashima, M. Inase, R. Kajiwara, M. Shinoda, T.Takahashi, K.Tsukada, H.Hirose and K. Niisato, “Real-time optical imaging provides dynamic map of brain activity,” The 5th International conference on neural information processing (ICONIP ‘98), pp. 329-332, 1998
15. M. Inase, T. Iijima, I. Takashima, T. Takahashi, M. Shinoda, H. Hirose, K. Niisato, K. Tsukada, “Optical recording of the motor cortical activity during reaching movement in the behaving monkey,” Society for Neuroscience Abstracts, Vol.24, 158.11, 1998

High-speed videography system using a pair of imagers for biological applications

Riichi Kajiwara, Ichiro Takashima, Kiyo Murano, Yuka Mimura, and Toshio Iijima

Supermolecular Science Division, Electrotechnical Laboratory,
1-1-4 Umezono, Tsukuba, Ibaraki 305-8568 Japan

ABSTRACT

This paper describes a high-speed imaging system using dual MOS-based solid-state cameras and its biological application. Our dual camera system can capture images synchronously and produce sets of 64 × 64-pixel images at a rate of 0.6 ms/frame. The system is composed of three blocks: the "camera-drive", "memory", and "processor" blocks. We developed these block hardware circuits using an FPGA device in the following manner. (1) Camera-drive block: two cameras were synchronized with the Hd (horizontal drive) and Vd (vertical drive) signals using a 16 MHz clock. (2) Memory block: 12-bit track-and-hold A/D converters were used to digitize the output from both cameras in parallel and store it in frame memory. Each camera had a 16-MB memory capacity. (3) Processor block: image data from both cameras was stored in two separate frame memories. This block simultaneously accessed the same memory address for each frame and calculated the difference in the observed values, which was then transferred to a personal computer. This system enabled us to observe pure neural activity from images contaminated with heartbeat noise.

Keywords: voltage-sensitive dye, fluorescence, optical recording, neural activity, pulsation noise, MOS-based solid state camera

1. INTRODUCTION

In biological studies and particularly in neural measurements, it is advantageous to observe the electrical activity of individual neurons without the use of an electrode. Several optical recording systems using fluorescent probes have been developed for this. In 1968, Cohen et al.[1] reported the discovery of changes in the optical properties of axons that occur during the action potential. In 1973, Davalia et al. [2] were able to measure the action potential of a giant axon by staining it with a merocyanine dye, which produced a detectable fluorescence change. That same year, they also detected the action potential of individual sensory neurons from leech segmental ganglia, in which the cell body was only 68 μm in diameter[3]. In 1981, Grinvald[4] developed optical monitoring methods for multiple site activity along the nerve cell processes in a culture.

In order to image electrical activity optically, the preparation under study is first stained with a suitable voltage-sensitive dye. The dye molecules bind to the external surface of excitable membranes and act as molecular transducers that transform change in the membrane potential into optical signals. These optical signals originate from electrical-activity-dependent changes in the absorption or emitted fluorescence of the dye, which respond in microseconds. These changes are linearly correlated with changes in both the membrane potential and stained membrane area. The resulting changes in absorption or the emitted fluorescence are then monitored with light-measuring devices. An array of photodetectors is positioned in the microscope image plane to simultaneously detect the electrical activity of several targets. Optical imaging with voltage-sensitive dye permits the visualization of neural activity with a sub-millisecond time resolution and a spatial resolution of 50-100 microns. The instrumentation must be able to record these fast optical signals with high spatial resolution over a large area. The apparatus required to accomplish this must include a fast camera (300 to 2000 Hz) along with elaborate data acquisition software, and display and analysis hardware. The first camera systems were 10 × 10- or 12 × 12-element photodiode matrix arrays that could perform multiple-site fast optical recording[5, 6]. Since then, higher spatial-temporal resolution and better signal-to-noise ratios have been achieved using 16 × 16-, 22 × 22-, 24 × 24-, and 34 × 34-element photodiode arrays[7, 8]. While photodiode array sensors have high temporal resolution because of their parallel readout method, their spatial resolution is intrinsically limited. In contrast to photodiode arrays, a CCD camera has high spatial resolution (several hundred pixels in each dimension), but poor temporal resolution due to its serial readout scheme. Therefore, CCD cameras are typically used for intrinsic signal optical imaging to visualize discrete functional modules of

the cortex, since the slow speed of intrinsic signals (rise time >1 s) allows commercially available CCD cameras (capturing several frames / s) to be used for intrinsic signal imaging[9, 10]. Some researchers, however, have increased CCD speed by utilizing spatial integration on the CCD chip and have used this process for fura-2 fluorescence imaging and voltage-sensitive dye recording[11-13]. This type of CCD operates at a reduced spatial resolution in exchange for a higher frame rate.

We developed an MOS-based monolithic array camera (128 × 128 elements) with a temporal resolution of 0.6 ms[14]. More recently, Takashima et al. (1999) developed a CCD system with millisecond time resolution to trace the dynamics of neural action potentials that cover a wide cortical area with sufficient spatial resolution[15]. For biological applications, high-speed CCD systems have an advantage over MOS-based systems since CCD systems require about 1/3 the imaging illumination intensity. This implies that CCD's are more suitable for long records (> than 10 seconds). However, the signal to noise ratio of an MOS-system (77 dB) is much better than that of a CCD system (65 dB), implying that MOS-systems are only more useful for measuring fast neural activity. MOS-imaging systems have already successfully imaged neuronal activity in rat hippocampal slices[16, 17], entorhinal–hippocampal slices[18], and an isolated guinea pig brain[19]. However, MOS-systems may require post-signal processing in cases where the images were contaminated with pulsation noise *in vivo*. This is especially significant when the voltage-sensitive dye RH-795 (maximum excitation wavelength of 530 nm) is used, as the heartbeat artifact noise cannot be ignored[20].

To circumvent this problem, we have developed a dual-camera imaging system. Sinha et al. [21] reported their results using a photodiode array for biological applications using a dual-camera fast optical recording system. They measured different biological signals with separate emission-wavelengths (voltage response and calcium influx). The dual-camera system also improved the image quality obtained during the study. For example, light source fluctuations could be reduced by subtracting the noise component detected in one camera from the signals detected by the other camera. During the simultaneous recording of membrane voltage and calcium influx using laser-scanning microscopy, Bullen and Saggau[22] were able to reduce light source noise using this concept. Our dual-camera high-speed imaging system enabled real-time visualization of different activities, such as (1) heartbeat biological noise and (2) neural activity contaminated with heartbeat noise. The subtraction of these two signals made it possible to reduce biological noise. Our system was able to obtain pure neural activity using the following three steps, which were processed simultaneously. (1) Camera 1 collected images containing both neural activity and the heartbeat artifact; (2) Camera 2 recorded only the heartbeat artifact component, and (3) the heartbeat artifact was removed by subtracting the Camera 2 images from the Camera 1 images. This paper describes the imaging system that we designed, with two MOS image sensors, and presents experimental data.

2. CAMERA ARCHITECTURE[14]

2.1. MOS-based Solid-State Camera

A schematic structure of an MOS-based solid-state sensor (FS 4361, Fuji Photo Film Co., Tokyo, Japan) is illustrated in Fig. 1. An array of 128 × 128 photodiodes and switching MOS field effect transistors (MOS-FETs) was fabricated on the chip. Each pixel had a 70 × 70-μm^2 area for light reception that was converted to an electrical charge. The sensor had eight parallel signal output lines in order to improve output speed. A 4-MHz (250-ns) clock pulse was used to achieve a sampling period per picture of 0.6 ms. In our optical imaging experiments, pixels were binned in 2 × 2 blocks in order to enhance sensitivity, which resulted in 64 × 64-pixel images.

The size of the pixel surface area limits the signal-to-noise ratio because the size determines the photo-charge that can accumulate in the diode capacitance. Theoretical considerations predict that the signal-to-noise ratio will exceed 77 dB for a pixel size of 70 × 70 μm^2. However, we found that the signal-to-noise ratio of the output photo-signal was about 70 dB, and this was caused mainly by an increase in amplifier noise. This was quite satisfactory, since the absorption or fluorescence light accompanying neural activity may vary by a factor of 10^{-2} – 10^{-4}, while the light intensity steadily illuminates the neural circuit[23, 24]. The camera unit was small (5 × 5 × 12 cm) and lightweight (200 g) and could be attached to the optical apparatus with a C mount adapter, as shown in Fig. 2.

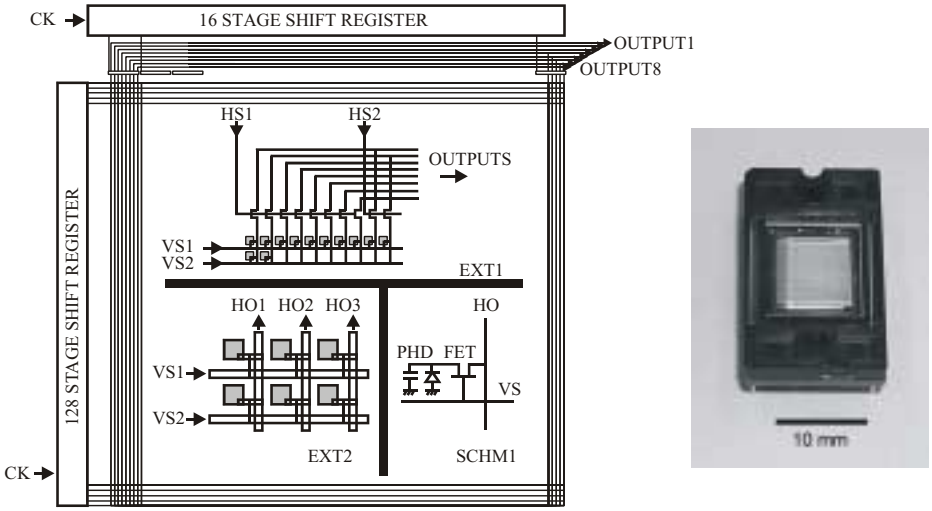

Fig.1. Schematic of a 128 × 128-pixel sensor and a photograph of the sensor chip. CK, clock; HS, horizontal shift; VS, vertical shift; HO, horizontal output; PHD, photodiode; FET, field-effect transistor. Insert 1, Horizontal scanning matrix; Insert 2, Arrangement of PHD; Insert 3, Peripheral photodiode circuitry.

Fig. 2. Photograph of the camera unit. The size of the camera is similar to that of a package of cigarettes.

2.2. Background Image Subtraction Circuit

In our optical imaging study, we observed and recorded the relative changes in light intensity, instead of the absolute light intensity, because fractional change in dye epifluorescence is associated with changes in the trans-membrane potential of the neuron ensemble.

A custom circuit (Fig. 3) was designed and incorporated into our system. This circuit was necessary because it was impossible to obtain an analog-to-digital converter (ADC) that had a fast conversion time (500 ns) along with a high bit number (> 14 bits). For physiological purposes, the sampling period per 64 × 64-pixel image should be in the sub-millisecond range. We choose a period of 512 μs, which then required using a 2-MHz (500-ns) clock pulse as the horizontal shift register trigger. In Figure 3, we first activated the write-mode (selector switch to A in Fig. 3) so that the sensor analog signal output was sent to an ADC (8 bit, 500 ns, ADS-132MC, Datel Inc., Mansfield, MA) and then stored in memory (SRAM). Once the reference signal for each pixel was stored in memory, we could then monitor any optical changes by setting an internal switch to read-mode (selector switch to B in Fig. 3). This allowed the input to be compared to the corresponding pixel's reference signal, which was recalled from memory and passed through a digital-to-analog converter (DAC). The difference between signals was amplified and allowed us to determine any fractional change in the photo-signals. This circuit, in combination with an ADC and DAC (1% accuracy), enabled us to obtain an amplification factor of 30. Based on this, we used three serial stages of these custom circuits to obtain an overall amplification factor of 10^3.

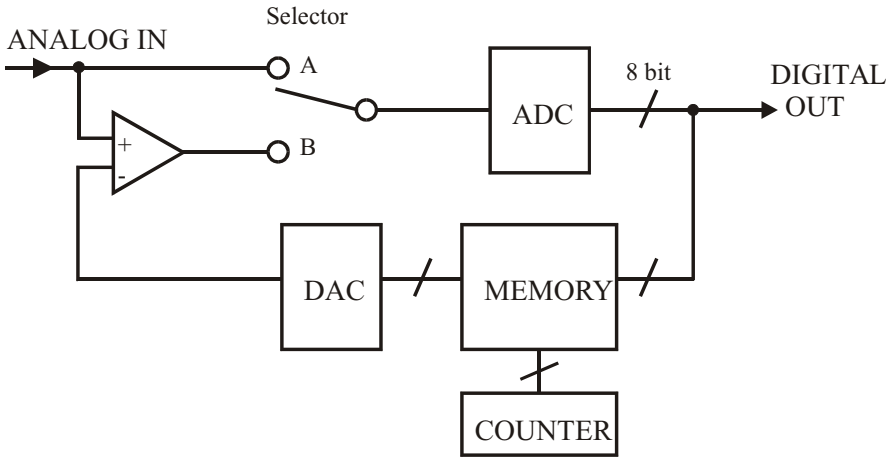

Fig. 3. Custom circuit for differential amplification of input and reference signal.

3. DUAL-IMAGE SYSTEM

3.1. Construction of the Dual-Camera System

The construction of our dual-MOS-camera system is shown in Fig. 4; it was based on previously developed imaging systems[14]. We developed the hardware circuit that drove both cameras and calculated the signal difference from both cameras. Our system was composed of three blocks: the "camera-drive", "memory", and "processor" blocks. We developed the block hardware circuit with an FPGA device (FLEX10K50VBC356-1, ALTERA Co., San Jose, CA) as follows. (1) Camera-drive block: both cameras were synchronized with the Hd (horizontal drive) and Vd (vertical drive) signals using a 16-MHz clock source. (2) Memory block: 12-bit track-and-hold A/D converters were utilized and the output from both cameras was digitized in parallel and stored in frame memory. Each camera had a 16-MB memory capacity. (3) Processor block: image data from both cameras was stored in two separate frame memories. This block simultaneously accessed the same memory address for each frame and calculated the difference. The difference data were then transferred to a personal computer.

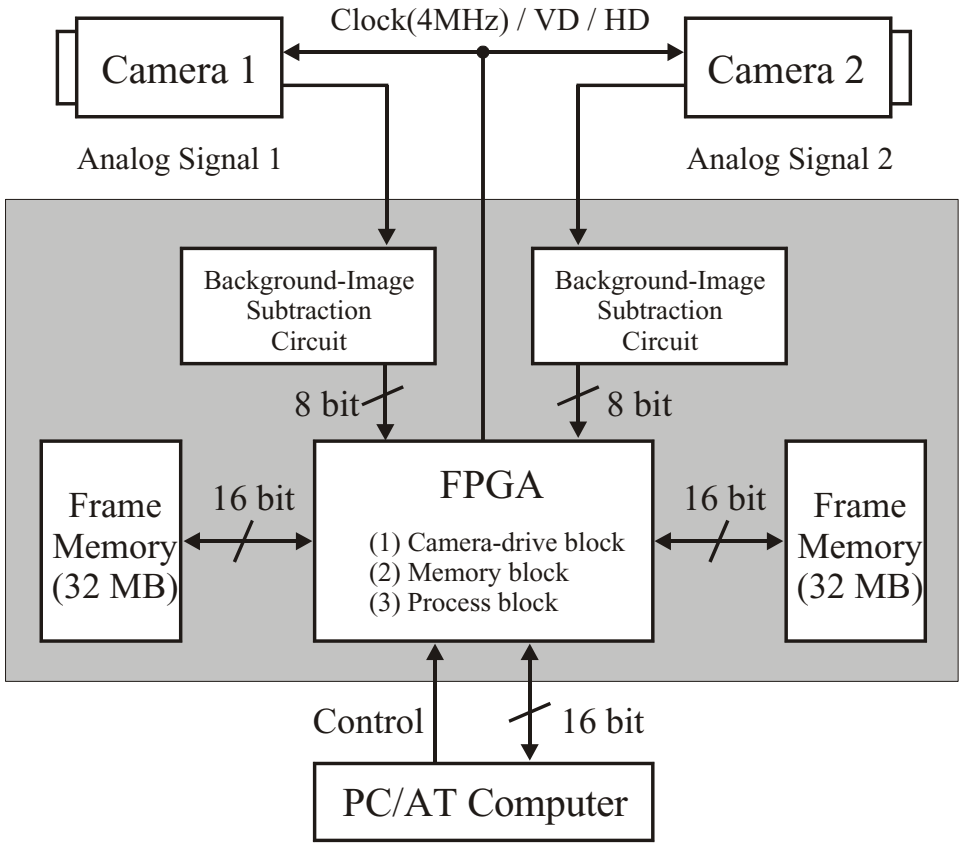

Fig. 4. Block diagram of the dual-camera system

3.2. Optical Apparatus

The optical apparatus, constructed in our laboratory, is similar to the tandem type epi-fluorescent microscope of Ratzlaff and Grinvald[25]. We used custom-made f =50 mm F/1.2 lenses for the first objective and f =100 mm lenses for the second objective, resulting in 2× magnification. The voltage-sensitive dye RH-795 has excitation and emission maxima at 530 and 712 nm, respectively. Illumination from a filtered (535 ±20 nm bandpass) voltage-stabilized tungsten–halogen lamp is guided to the preparation by an optical fiber. The cameras are attached to a microscope in which two optical paths branch via a half mirror. Optical filters with different band-pass characteristics are placed just before each camera (Fig. 5). We used a band-pass filter for the dye emission wavelengths (emission filter) and another for wavelengths that were insensitive to neural activity (reference filter). The emission filter was a red long-wavelength pass filter (50% transmittance at 605 nm; Kodak wratten filter, No. 26) and the reference filter was a green band-pass filter (530±30 nm; Kodak wratten filter, No. 58). Use of a 60 -40% half mirror (60% optical path for the red filter, 40% for the green) resulted in nearly equal intensities of the fluorescent and reflected light, as measured by the cameras. Our dual camera system has the ability to capture images synchronously and produce sets of 64 × 64-pixel images at a rate of 0.6 ms/frame.

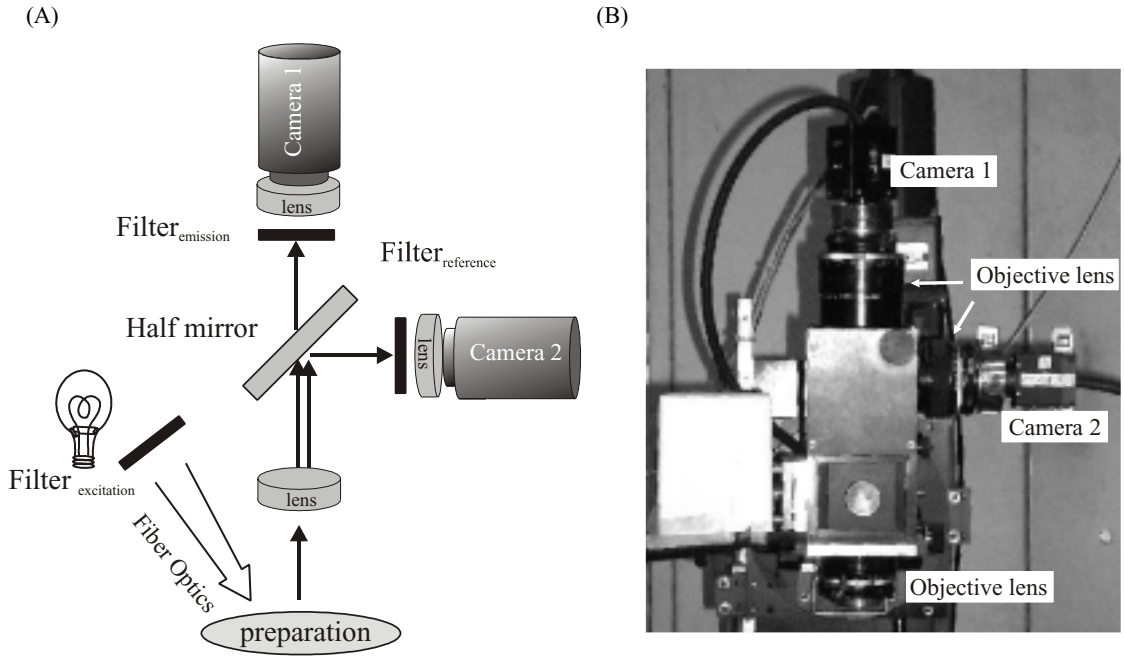

Fig. 5. (A) Schematic illustration and (B) photograph of the optical apparatus.
The halogen lamp and fiber optics are not shown in the photograph.

4. BIOLOGICAL APPLICATION

4.1. Neural Activity in Rat Somatosensory Cortex

In vivo experiment: we stained the cortex of male Wistar rats (~ 300 g) with a voltage-sensitive dye and obtained images of neural activity. The preparation and maintenance methods for the animals were similar to previously described protocols[15]. Each animal was anesthetized with an intraperitoneal injection of ketamine (80 mg/kg) / xylazine (8.8 mg/kg). The animal was positioned in a stereotaxic head-holder. A well of dental acrylic was built around the exposed cortex. After removing the dura matter, the cortical surface was stained with a voltage-sensitive dye RH-795 (Molecular Probes, 0.6 mg/ml) for one hour. The dye was then completely washed out and the well was filled with artificial cerebrospinal fluid (ACSF: 125 mM NaCl, 5 mM KCl, 2 mM $CaCl_2$, 1.25 mM $MgSO_4$, 1.25 mM NaH_2PO_4, 22 mM $NaHCO_3$, and 10 mM glucose). The animal was placed under the optical apparatus as shown in Fig. 5.

Electrical stimulation (200 μs in duration, 40V in intensity) was applied to the left whisker pads of the snout. In the optical imaging experiments, dye epifluorescence was detected by the imaging system, which was synchronized with the heartbeat, and its fractional change was calculated. Electrical stimulation was applied 900 ms after acquisition began. Figure 6 shows evoked neural activity in the somatosensory cortices. Camera 1 measured the fluorescence of neural activity contaminated with heartbeat noise. Camera 2 measured only the heartbeat noise. The pulsation noise was subtracted using our hardware system. In some staining conditions, the ratio of fluorescence ($\Delta F_{camera1}/\Delta F_{camera2}$) did not equal 1. In such cases, we compensated for varying signal strength before subtraction in the "processor block" in the FPGA (Fig. 4).

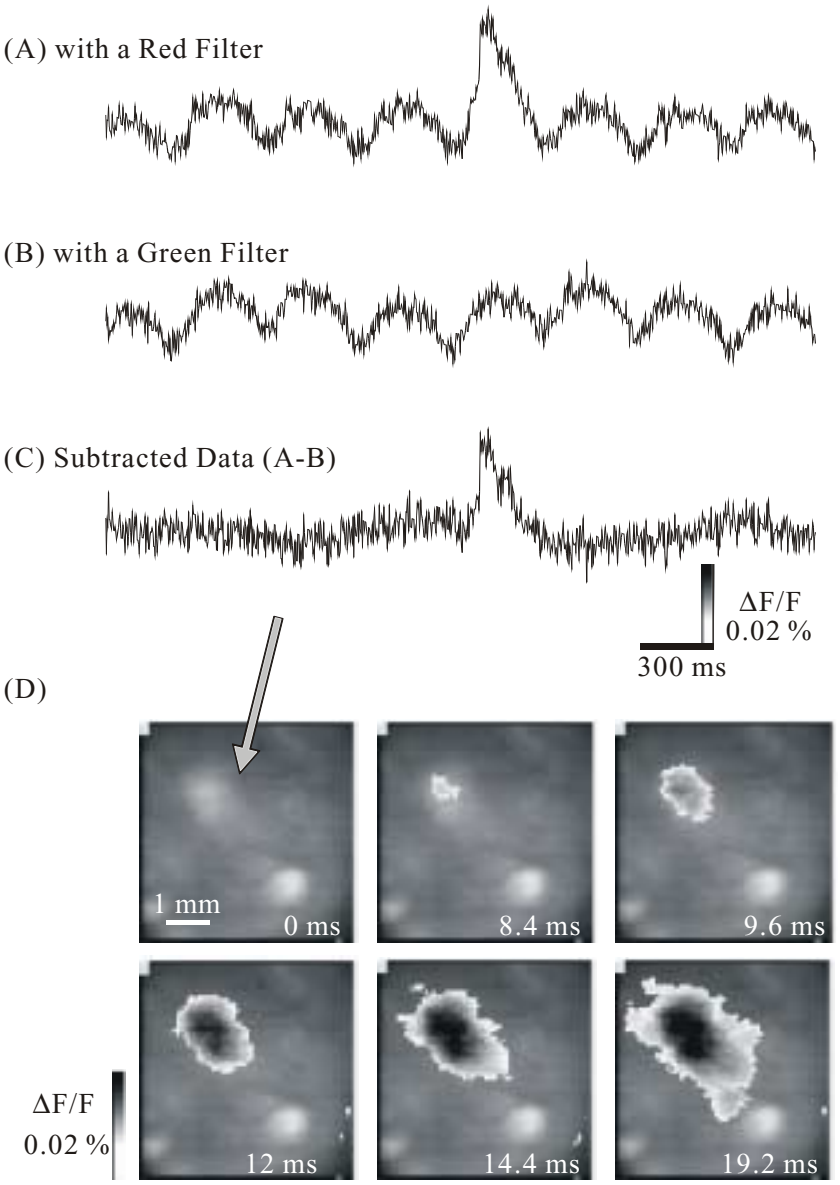

Fig.6. *In vivo* optical imaging of evoked neural activity in the rat somatosensory cortex.

The data was 16-times averaged. (A) Optical signal trace in a pixel (indicated by an arrow in (D)) as measured by Camera 1 with a red filter. (B) Optical signal trace in the same pixel as measured by Camera 2 with a green filter. (C) Subtracted optical signal trace ((A) – (B)). (D) Real-time imaging of the difference data (C). The time after electrical stimulation start is indicated on each image. Depolarization was measured as the fractional changes in each pixel's fluorescence (ΔF/F). This value is encoded in "pseudocolor " as indicated in the scale, and is superimposed on a morphological image of the preparation. The neural activity in the somatosensory cortex was evoked by whisker pad stimulation.

CONCLUSIONS

We developed an optical imaging system using dual MOS-based solid-state cameras for use in biological applications. We incorporated hardware circuitry into our system in order to drive both cameras and calculate differences in the measured image data. Our dual-camera system has the ability to capture images synchronously and produce sets of 64 × 64-pixel images at a rate of 0.6 ms/frame. Our dual camera system dramatically reduced the pulsation noise in the rat *in vivo* experiments. In summary, we observed and recorded accurate images of neural activity using the following three simultaneous processes: (1) Camera 1 collected images reflecting both neural activity and heartbeat artifact, (2) Camera 2 recorded only the heartbeat artifact, and (3) the heartbeat artifact was subtracted from the Camera 1 images.

ACKNOWLEDGEMENTS

We thank Dr. M. Ichikawa at Riken for technical advice regarding the optical system with MOS-image sensor. This work was supported by the Agency of Industrial Science and Technology (AIST) of Japan, Japan Science and Technology Corporation (JST).

REFERENCES

1 L.B. Cohen, R.D. Keynes and B. Hille, "Light scattering and birefringence changes during nerve activity", Nature, **218**, pp. 438-441, 1968

2 H.V. Davila, B.M. Salzberg, L.B. Cohen and A.S. Waggoner, "A large change in axon fluorescence that provides a promising method for measuring membrane potential", Nat New Biol, **241**, pp. 159-160, 1973

3 B.M. Salzberg, H.V. Davila and L.B. Cohen, "Optical recording of impulses in individual neurones of an invertebrate central nervous system", Nature, **246**, pp. 508-509, 1973

4 A. Grinvald and I.C. Farber, "Optical recording of calcium action potentials from growth cones of cultured neurons with a laser microbeam", Science, **212**, pp. 1164-1167, 1981

5 A. Grinvald, L. Anglister, J.A. Freeman, R. Hildesheim and A. Manker, "Real-time optical imaging of naturally evoked electrical activity in intact frog brain", Nature, **308**, pp. 848-850, 1984

6 B.M. Salzberg, A.L. Obaid, D.M. Senseman and H. Gainer, "Optical recording of action potentials from vertebrate nerve terminals using potentiometric probes provides evidence for sodium and calcium components", Nature, **306**, pp. 36-40, 1983

7 T. Iijima, G. Matsumoto and Y. Kidokoro, "Synaptic activation of rat adrenal medulla examined with a large photodiode array in combination with a voltage-sensitive dye", Neuroscience, **51**, pp. 211-219, 1992

8 M. Nakashima, S. Yamada, S. Shiono, M. Maeda and F. Satoh, "448-detector optical recording system: development and application to Aplysia gill-withdrawal reflex", IEEE Trans Biomed Eng, **39**, pp. 26-36, 1992

9 D.Y. Ts'o, R.D. Frostig, E.E. Lieke and A. Grinvald, "Functional organization of primate visual cortex revealed by high resolution optical imaging", Science, **249**, pp. 417-420, 1990

10 R.D. Frostig, E.E. Lieke, D.Y. Ts'o and A. Grinvald, "Cortical functional architecture and local coupling between neuronal activity and the microcirculation revealed by in vivo high-resolution optical imaging of intrinsic signals", Proc Natl Acad Sci U S A, **87**, pp. 6082-6086, 1990

11 N. Lasser-Ross, H. Miyakawa, V. Lev-Ram, S.R. Young and W.N. Ross, "High time resolution fluorescence imaging with a CCD camera", J Neurosci Methods, **36**, pp. 253-261, 1991

12 C. Cabo, A.M. Pertsov, W.T. Baxter, J.M. Davidenko, R.A. Gray and J. Jalife, "Wave-front curvature as a cause of slow conduction and block in isolated cardiac muscle", Circ Res, **75**, pp. 1014-1028, 1994

13 P. Gogan, I. Schmiedel-Jakob, Y. Chitti and S. Tyc-Dumont, "Fluorescence imaging of local membrane electric fields during the excitation of single neurons in culture", Biophys J, **69**, pp. 299-310, 1995

14 M. Ichikawa, T. Iijima and G. Matsumoto, "Real-time optical recording of neuronal activities in the brain." In: *Brain mechanisms of perception and memory*, T. Ono, L.R. Squire, M.E. Raichle, D.I. Perrett and M. Fukuda , pp. 638-648, Oxford UP, New York, 1993

15 I. Takashima, M. Ichikawa and T. Iijima, "High-speed CCD imaging system for monitoring neural activity in vivo and in vitro, using a voltage-sensitive dye", J Neurosci Methods, **91**, pp. 147-159, 1999

16 M.E. Barish, M. Ichikawa, T. Tominaga, G. Matsumoto and T. Iijima, "Enhanced fast synaptic transmission and a delayed depolarization induced by transient potassium current blockade in rat hippocampal slice as studied by optical recording", J Neurosci, **16**, pp. 5672-5687, 1996
17 Y. Otsu, E. Maru, H. Ohata, I. Takashima, R. Kajiwara and T. Iijima, "Optical recording study of granule cell activities in the hippocampal dentate gyrus of kainate-treated rats", J Neurophysiol, **83**, pp. 2421-2430, 2000
18 T. Iijima, M.P. Witter, M. Ichikawa, T. Tominaga, R. Kajiwara and G. Matsumoto, "Entorhinal-hippocampal interactions revealed by real-time imaging", Science, **272**, pp. 1176-1179, 1996
19 M. de Curtis, I. Takashima and T. Iijima, "Optical recording of cortical activity after in vitro perfusion of cerebral arteries with a voltage-sensitive dye [In Process Citation]", Brain Res, **837**, pp. 314-319, 1999
20 D. Shoham, D.E. Glaser, A. Arieli, T. Kenet, C. Wijnbergen, Y. Toledo, R. Hildesheim and A. Grinvald, "Imaging cortical dynamics at high spatial and temporal resolution with novel blue voltage-sensitive dyes", Neuron, **24**, pp. 791-802, 1999
21 S.R. Sinha, S.S. Patel and P. Saggau, "Simultaneous optical recording of evoked and spontaneous transients of membrane potential and intracellular calcium concentration with high spatio-temporal resolution", J Neurosci Methods, **60**, pp. 49-60, 1995
22 A. Bullen and P. Saggau, "Indicators and optical configuration for simultaneous high-resolution recording of membrane potential and intracellular calcium using laser scanning microscopy", Pflugers Arch, **436**, pp. 788-796, 1998
23 A. Grinvald, L.B. Cohen, S. Lesher and M.B. Boyle, "Simultaneous optical monitoring of activity of many neurons in invertebrate ganglia using a 124-element photodiode array", J Neurophysiol, **45**, pp. 829-840, 1981
24 L.B. Cohen, B.M. Salzberg, H.V. Davila, W.N. Ross, D. Landowne, A.S. Waggoner and C.H. Wang, "Changes in axon fluorescence during activity: molecular probes of membrane potential", J Membr Biol, **19**, pp. 1-36, 1974
25 E.H. Ratzlaff and A. Grinvald, "A tandem-lens epifluorescence macroscope: hundred-fold brightness advantage for wide-field imaging", J Neurosci Methods, **36**, pp. 127-137, 1991